1 **Flow regulates biological NO_3^- and N_2O production in a turbid sub-tropical stream**

2

3

4 Naomi S. Wells[1*], Bradley Eyre[1]

5

6

7

8

9 [1] Centre for Coastal Biogeochemistry, School of Environment, Science & Engineering,

10 Southern Cross University, PO Box 157, East Lismore, 2480 NSW, Australia

11

12 *Author for correspondence: naomi.wells@scu.edu.au

13

15

16

17

18

19

20

21

22

23

24

25

26 **Abstract**

27   Streams play a critical role in attenuating the excess reactive nitrogen generated from

28 human activities. These systems can consequently also emit significant amounts of N_2O, a

29 potent greenhouse gas. Models and manipulative experiments now suggest that hydrology

30 regulates the balance between nitrogen removal and N_2O production. We aimed to

31 empirically test this hypothesis by measuring changes in the concentration and isotopic

32 composition of NO_3^- ($\delta^{18}O$, $\delta^{15}N$) and N_2O ($\delta^{18}O$, $\delta^{15}N$, site preference) in hyporheic

33 sediments and surface water of a 30 m reach over eight days of falling stream discharge (2.7

34 to 1.8 m^3 s^{-1}). The stream was persistently heterotrophic (productivity/respiration: 0.005 -

35 0.2), while changes in conductivity, $\delta^{18}O$-H_2O, and ^{222}Rn indicated that hyporheic mixing

36 decreased and net groundwater inputs increased as discharge declined. The shallow

37 groundwater had high inorganic N concentrations (2 – 10 mg l^{-1}), but increased groundwater

38 inputs could not fully explain the concurrent increases in NO_3^- (1 – 3 mg N l^{-1}) and N_2O (700

39 to 1000 % saturation) in the surface water. Biologically, rather than solely hydrologically,

40 regulated stream nitrogen export was confirmed by changes in N_2O and NO_3^- isotopic

41 composition. However, isotope patterns indicated that nitrification, not denitrification,

42 increased surface water NO_3^- and N_2O concentrations as hyporheic exchange decreased.

43 These findings empirically demonstrate how flow dynamics regulate biological NO_3^-

44 production as well as transport, with implications for predicting aquatic N_2O emissions.

45

46 **Keywords:** stable isotopes, isotopomers, hyporheic zone, surface water – groundwater

47 interactions, freshwater tidal zone, sub-tropics

48

49

50

1. Introduction

Excess reactive nitrogen (N) generated from human activities like agriculture and fossil fuel combustion causes a range of environmental damages, from biodiversity loss through to global climate change (Fowler et al., 2013; Galloway et al., 2008). Streams and rivers play a critical role in regulating these damages as they determine the form and quantity of N transported from land to sea (Boyer et al., 2006; McCrackin et al., 2014; Tysmans et al., 2013). However, the same conditions that maximise reactive N removal may also promote the release of nitrous oxide (N_2O), an ozone depleting greenhouse gas with 298 times the warming potential of carbon dioxide (CO_2) (Alexander et al., 2009; Quick et al., 2019; Turner et al., 2015). Evaluations of the biological and hydrological controls on reactive N removal in streams must therefore be expanded to account for potential trade-offs with N_2O emissions.

At the global scale, waterways with higher surface water nitrate (NO_3^-) concentrations tend to emit more N_2O (Hu et al., 2016; Murray et al., 2015). However, it is not yet clear whether this correlation is causal, as within-reach studies frequently show decoupling of NO_3^- and N_2O fluxes (e.g., Comer-Warner et al., 2020b). This disconnect reflects the complexity of N cycling, which can be both assimilated and/or converted via dissimilatory microbial pathways through seven redox states. Nitrous oxide is an intermediate product of both microbial N oxidation (nitrification, $NH_3 \rightarrow NO_3^-$) and reduction (denitrification, $NO_3^- \rightarrow N_2$), plus other minor microbial processes (Quick et al., 2019). Positive correlation between NO_3^- and N_2O can thus be produced by either, 1) nitrification-limited N_2O and NO_3^- production, or, 2) NO_3^--limited denitrification producing N_2O.

Stream N_2O emissions are often assumed to come primarily from denitrification (Beaulieu et al., 2011; Rosamond et al., 2012). Typically O_2 saturated surface waters confine denitrification to anoxic zones in sediments and suspended particles (Reisinger et al., 2016; Seitzinger et al., 2006; Xia et al., 2017), so stream denitrification depends on both the extent

76 of anoxic zone formation (capacity) and efficiency of NO_3^- transport to these anoxic zones

77 (opportunity). Capacity is affected by C availability, sediment composition, and biological

78 productivity (Christensen et al., 1990; Covino et al., 2018; Eyre and Ferguson, 2009;

79 Trimmer et al., 2012). Stream hydrology controls the opportunity for N removal: slower flow

80 velocities increase time for reactions to occur (Alexander et al., 2009; Briggs et al., 2014;

81 Marcé et al., 2018), while vertical hyporheic zone surface water – groundwater mixing moves

82 NO_3^- through anoxic zones (Gomez-Velez et al., 2015; Krause et al., 2017). However, N_2O

83 fluxes are only inconsistently explained by denitrification capacity factors like NO_3^-

84 concentrations (Hu et al., 2016), NO_3^- consumption rates (Comer-Warner et al., 2020b;

85 Laursen and Seitzinger, 2004), or O_2 (Baulch et al., 2012; Clough et al., 2007; Reading et al.,

86 2017; Rosamond et al., 2011; Wu et al., 2018). New models propose overcoming these

87 inconsistencies by focusing on hydrology (opportunity). These predict that stream N_2O is

88 highest under unstable or intermediate flow conditions, when N_2O is stripped from anoxic

89 NO_3^- reduction zones before it can be reduced to N_2 (Marzadri et al., 2017; Quick et al.,

90 2016). This fits with growing evidence that both opportunity and capacity must be accounted

91 for to predict assimilatory stream N removal (Covino et al., 2018). Yet difficulty quantifying

92 the hyporheic dynamics underpinning redox-dependent N cycling means large uncertainties

93 persist in estimates of both stream NO_3^- removal and N_2O emissions (Hampton et al., 2020).

94   The aim of this study was to empirically test whether the same mechanisms control

95 stream export of NO_3^- and N_2O. Dropping stream flow during a diurnal metabolism study

96 provided a unique opportunity to test the hypothesis that opportunity (hydrology), more than

97 capacity (biology), regulates stream N_2O emissions and NO_3^- removal. We measured changes

98 in the concentration and natural abundance isotopic composition of NO_3^- and N_2O in the

99 surface waters and porewaters (5 cm depth and 20 cm depth) of a stream both during the

100 night v day (changing capacity) and over time as the stream height fell (changing

101   opportunity). This approach is based on evidence that nitrification and denitrification

102   systematically discriminate against light isotopes (Boshers et al., 2019; Casciotti et al., 2003;

103   Granger and Wankel, 2016) so that NO_3^- isotopic composition ($\delta^{18}O$, $\delta^{15}N$) reflects stream N

104   cycling (Cohen et al., 2012; Wells et al., 2016). Similarly, N_2O isotopes ($\delta^{15}N$, $\delta^{18}O$) and

105   isotopomers (intramolecular site preference of ^{15}N, SP) help constrain the relative influence

106   of NO_3^- reduction, NH_3 oxidation, and N_2O reduction on N_2O fluxes (Ostrom and Ostrom,

107   2017; Well et al., 2012).

108

109   **2. Materials & Methods**

110   2.1 Site description

111   The study was carried out in Monaltrie / Gundurimba Creek, which drains into the

112   Wilson River in Lismore, New South Wales, Australia (28°50'57"S, 153°16'27"E) (Fig. 1).

113   The stream is tidal with muddy sediments. The site is underlain by fractured basalt, including

114   unconfined shallow aquifers, and sharp topography constrains water flow paths (Brodie et al.,

115   2007; Brodie et al., 2003). The region has a semi-tropical climate with warm, wet summers

116   and cool, dry winters, with mean temperatures ranging from 13°C to 28°C. Mean annual

117   rainfall is 1,200 mm rain. Effluent from a nearby wastewater treatment plant (WWTP)

118   discharges into Monaltrie Creek and the shallow groundwater upstream from the study site

119   (Fig. 1), leading to elevated DIN concentrations in both the surface and groundwater (Table

120   1). Local shallow groundwater is ~21°C and the surface water between 19 and 27 °C.

121

122   2.2 Experimental design

123   Surface water (*SW*), surface sediment porewaters (*S*), and hyporheic zone water (*HZ*)

124   were sampled at nine locations across a 30 m stream reach over five 24 h periods spanning

125   eight days in April 2017 (late summer). We logged changes in N_2O, as well as supporting

126 chemical (O_2, CO_2, CH_4, conductivity) and hydrologic (radon, ^{222}Rn, as a proxy for

127 groundwater inputs, as well as temperature, flow velocity, and stream height) parameters

128 every 1 s^{-1} – 30 min^{-1} in the centre of the sampled reach. This intensive local sampling design

129 enabled us to identify 'hot spot' zones of surface water -groundwater interactions and directly

130 relate subsurface processes to temporal surface dynamics. Discrete samplings were timed to

131 the O_2 maxima and minima of each day in order to fully capture stream N variability (Baulch

132 et al., 2012; Christensen et al., 1990): samples were collected at 02:00 and 14:00 on D1, D2,

133 and D4, then at low and high tides for D6 and D8 after reviewing O_2 data. Climate data (wind

134 speed, air temperature, rainfall) was downloaded from the Bureau of Meteorology station

135 (http://www.bom.gov.au/climate/dwo/IDCJDW2074.latest.shtml, accessed 16/06/2017).

136

137 2.2.1 Discrete samples

138   Surface water samples were collected by filling a 1 L bottle and then sub-sampling

139 into vials using a 20 ml syringe (Fig. 1). For the surface sediments (*S*), diffusive equilibration

140 in thin-film (DET) probes were degassed for 8 hr in a 0.01M NaCl solution purged with N_2,

141 then installed to 5 cm depth six hours prior to sampling (Huang et al., 2016; Huang et al.,

142 2019). Probes were collected prior to the surface grab samples and stored wrapped in

143 cellophane. Hyporheic samples were collected from piezometers (20 cm internal diameter)

144 installed 20 cm below the sediment surface. A 50 ml syringe was used to collect *HZ* water,

145 with the first 50 ml discarded to purge the well. The *SW* and *HZ* samples were either passed

146 through 0.22 µm syringe tip filters (polyethersulfone, Minisart) for inorganic nutrient (PO_4^{3-},

147 NO_3^-, and NH_4^+) and NO_3^- dual isotope analyses, or passed through a 0.45 µm syringe tip

148 filter (polyethersulfone, Minisart) into a pre-combusted 40 ml glass vial sealed with a Teflon

149 septa for organic carbon (DOC) analysis. Samples were frozen at -20°C until analysis.

150 Additional surface water samples for δ^{15}N-N_2O, δ^{18}O-N_2O, and SP-N_2O were collected in

151 500 ml glass crimp-top bottles (Wheaton). These were stored in the dark at 4°C, and analysed

152 within one month of collection. Conductivity (Eutech Instruments) in *HZ* and *SW* samples,

153 and temperature and O_2 (Hach LDO) in *HZ* samples, were measured in the field prior to

154 filtering. The DET probes were cut along the sediment – surface water line, placed into a

155 sterile plastic vial, and frozen at -20°C until analysis.

156

157 2.2.2 Continuous measurements

158   Loggers were installed at B2 (Fig. 1). Flow velocity (*v*) and water depth (*h*) were

159 logged every 10 min using an ultrasonic Doppler instrument (Starflow, Unidata) placed on

160 the sediment surface, and water chemistry, including DO, logged every 30 minutes using a

161 Hydrolab HL4 installed 20 cm below the water surface. Other dissolved gasses (^{222}Rn, CO_2,

162 CH_4, and N_2O) were measured by continuously pumping water from 20 cm below the surface

163 through a showerhead exchanger (Durridge). Air from the exchanger was pumped through a

164 Drierite column to remove moisture, and then to either a Picarro G2308 (N_2O, CH_4), LI-COR

165 LI-820 (CO_2), or a Durridge RAD7 (^{222}Rn). Carbon dioxide and N_2O concentrations were

166 logged $\sim 1\ s^{-1}$ and ^{222}Rn every 10 min. Measurement precision was 0.05% for N_2O. Picarro

167 stability was confirmed prior to use using N_2 (0 ppm N_2O) and N_2O (28 ppm) gasses. The LI-

168 COR was calibrated prior to deployment (0 ppm, 1000 ppm), and had 1 ppm precision.

169

170 2.3 Sample analyses

171   Inorganic nutrient concentrations were measured using a Lachat Flow Injection

172 Analyser, see Eyre and Pont (2003) for details. Note NO_3^- was measured as $NO_3^- + NO_2^-$ and

173 NH_4^+ as $NH_3 + NH_4^+$. DOC concentrations were measured via continuous flow wet oxidation

174 on an Aurora 1030W TOC analyser. For *S* samples, DET gels were extracted overnight using

175   10 ml deionised water, which was then analysed for NO_3^- and NH_4^+ concentrations and NO_3^-

176   dual isotope composition (Comer-Warner et al., 2017; Huang et al., 2016).

177   Water isotopes ($\delta^{18}O$-H_2O) in *SW* and *HZ* samples was measured on a High

178   Temperature Conversion Elemental Analyzer (Thermo-Fisher TC-EA) coupled to an IRMS

179   (Thermo-Fisher Delta-V plus) via a Thermo-Fisher ConFlo IV. Samples were measured 5x (1

180   μL injection) to account for carryover, and calibrated using VSMOW2 ($\delta^{18}O$ = 0.0‰) and

181   SLAP2 ($\delta^{18}O$ = -55.5‰) standards. Dual NO_3^- + NO_2^- isotopes ($\delta^{15}N$ and $\delta^{18}O$) were

182   measured using a *Pseudomonas aureofaciens* culture genetically modified to block N_2O

183   reduction to quantitatively convert NO_x^- to N_2O (McIlvin and Casciotti, 2011). Sample

184   batches were prepared along with triplicate culture blanks and the internationally certified

185   standards USGS34, USGS32, and USGS35. The produced $\delta^{15}N$ and $\delta^{18}O$ composition of the

186   produced N_2O was measured using a Thermo Fisher Delta V Plus IRMS fitted with a custom

187   gas bench (Thermo Fisher Gasbench II). The isotopic composition of *SW* N_2O ($\delta^{15}N$-N_2O,

188    $\delta^{18}O$-N_2O, and SP, where SP = $^{\alpha}N$ - $^{\beta}N$) was measured after injecting a 50 ml helium

189   headspace into the 500 ml sample bottles, allowing samples to equilibrate for >2 hr, and

190   adjusting the gas bench for manual injection (Murray et al., 2018). Data were corrected

191   offline as described in Toyoda and Yoshida (1999), and calibrated from triplicate

192   measurements of three internationally-verified N_2O isotope standards (Mohn et al., 2014).

193

194   2.4 Data analysis

195   Analyses were carried out in R v 4.0 / R Studio v 1.3.959. Stream discharge (Q, m^3 s^{-1}

196   ) was calculated from the logged flow velocity (v, in m s^{-1}) and reach cross-sectional area

197   (width × h). Downstream discharge of DOC and NO_3^- was calculated as the measured

198   concentration (g m^{-3}) × Q (m^3 s^{-1}) for the 3 h around sample collection. Water chemistry

199   differences were determined using mixed models, with sample locations as repeated

200   measures, time and depth as continuous variables, and width and length locations as fixed

201   factors, using lmer4 and merTools (Bates et al., 2015; Knowles and Frederick, 2019). Due to

202   sample numbers, tests were run separately for each depth layer. Figures were generated with

203   ggplot2, patchwork, and ggpubr (Kassambara, 2020; Pedersen, 2019; Wickham, 2016).

204

205   2.4.1 Biogenic gasses

206   Gross primary productivity (GPP) and ecosystem respiration (ER) were estimated as

207   functions of light using a maximum likelihood estimation model from streamMetabolizer R

208   (Appling et al., 2018). Estimates were based on measured O_2 concentrations, water

209   temperatures, Q, h, and the estimated solar radiation for the location × time.

210   N_2O, CO_2, and CH_4 data were block-averaged at 1 min^{-1} intervals, and dissolved

211   concentrations calculated based on the partial pressure (µatm) and solubility (K_0, in mol atm^{-1}

212   l^{-1}) calculated for each gas for a given temperature and conductivity. Dissolved ^{222}Rn

213   concentrations (dpm l^{-1}) were calculated as per Santos et al. (2012), dissolved N_2O (µg N l^{-1})

214   using the K_0 defined in Weiss and Price (1980), and CO_2 (mg l^{-1}) as per Wanninkhof (2014).

215   Time-lags created by variable gas equilibration times were applied to the data using values

216   previously calculated for this sampling set-up (15 min for N_2O and CO_2, 30 min for ^{222}Rn)

217   (Erler et al., 2015; Maher et al., 2013; Santos et al., 2012). The transfer velocity between the

218   surface water and air (k), which is regulated by v and h (Hall and Ulseth, 2019), was

219   calculated for each 1 min of data using three of the empirical equations outlined in (Raymond

220   et al., 2012) and used to calculate mean daily water-to-air N_2O fluxes (Suppl. Mat. 1).

221   Dissolved N_2O isotope and isotopomer values were corrected for mixing with

222   atmospheric N_2O to ensure that variations in concentrations did not bias the data, as

223   suggested by (Thuss et al., 2014). This was done using a two-pool mixing model (Eq. 1):

224   (Eq. 1) $\delta_{measured} = f_{air}\delta_{air} + f_{stream}\delta_{stream}$

225 $$1 = f_{air} + f_{stream}$$

226 where f_{air} is defined based on N_2O saturation, making this a conservative estimate of two-way

227 air-water mixing (Eq. 2):

228 (Eq. 2) $$f_{air} = \frac{0.32 \times K_0}{N2O_{measured}}$$

229 where 0.32 is the partial pressure of N_2O in the air and $N_2O_{measured}$ is the measured partial

230 pressure dissolved in the surface water. We then solved Eq. 1 assuming that 'air' N_2O had the

231 concentration and isotopic composition of tropospheric N_2O: $\delta^{15}N\text{-}N_2O$ = 7.0 ‰, $\delta^{18}O\text{-}N_2O$ =

232 43.7 ‰, SP = 18.7 ‰ (Yoshida and Toyoda, 2000). Dissolved $\delta^{18}O\text{-}N_2O$ values were

233 normalised to surface water $\delta^{18}O\text{-}H_2O$ values (Lewicka-Szczebak et al., 2017), to correct for

234 O exchange during N_2O production (Snider et al., 2009; Snider et al., 2013).

235

236 2.4.2 Surface water – groundwater interactions

237 Two approaches helped constrain surface water – groundwater mixing. First, the

238 proportion of surface water in the hyporheic zone was estimated from conductivity (Eq. 3):

239 (Eq. 3): $$f_{sw} = \frac{C_{GW} - C_{HZ}}{C_{GW} - C_{SW}}$$

240 where conductivity measured in sub-surface wells (C_{HZ}) is compared to the range of

241 conductivity range reported for shallow site groundwater (C_{GW}; Table 1) and measured in the

242 surface water (C_{SW}). Eq. 3 was solved for each sampling point using the mean ± SD of each

243 parameter. Second, the measured diurnal ^{222}Rn fluctuations were used to approximate

244 groundwater inputs to the surface water. This approach is based on the knowledge that

245 relatively short surface water ^{222}Rn residence times mean that measured concentrations must

246 come from subsurface inputs (Burnett et al., 2010; Khadka et al., 2017). The groundwater

247 flux into the surface water (Q_{GW}, in m^3 s^{-1}) was estimated by mass balance (Eq. 4):

248 (Eq. 4): $$Q_{GW} = \frac{F_{decay} + F_{air} + Q_{low}Rn_{low} - Q_{high}Rn_{high}}{Rn_{GW}}$$

249   where F_{decay} is [222]Rn removal due to radioactive decay and F_{air} is the [222]Rn water-air flux,

250   calculated using constants and parameterisations from Burnett et al. (2010), and the measured

251   differences between [222]Rn fluxes at low ($Q_{low} \times Rn_{low}$, in m^3 s^{-1} $\times$ dpm m^{-3}) and high ($Q_{high} \times$

252   Rn_{high}) tides approximate upstream [222]Rn inputs v. downstream exports, respectively. This

253   defines Q_{GW} as the [222]Rn flux not explained by hydrology. Eq. 4 was solved for each 24 h

254   sampling period using the maximum and minimum [222]Rn concentrations (230,000 dpm m^{-3}

255   and 20,000 dpm m^{-3} for local shallow groundwater (Atkins et al., 2013; Gatland et al., 2014).

256   Note that end-member uncertainty means that Eq. 3 and Eq. 4 help constrain, but do not

257   precisely quantify, changes in surface water – groundwater interactions over time.

258

259   **3. Results**

260   3.1 Hydrology

261   Stream height fluctuated tidally by ~0.1 m. Daily v peaks (up to ~2 m s^{-1}) coincided

262   dips in h minima (Fig. 2) and conductivity ($r = 0.4 – 0.7$, $p<0.001$). Surface water was 21 $\pm$

263   0.5 °C. Over time k_{600} values ranged from 1.3 $\pm$ 0.3 m d^{-1} to 0.73 $\pm$ 0.3 m d^{-1} (Suppl. Mat.

264   Table S1). Over time h declined from 1.1 to 0.86 m ($p<0.001$), Q decreased from 3 m^3 s^{-1} to

265   ~2 m^3 s^{-1} ($p<0.001$), and conductivity increased ($p<0.001$; Suppl. Mat. Table S3). Surface

266   water δ^{18}O-H_2O decreased over time (F = 17, $p<0.001$) (Table 2, Fig. 2). The [222]Rn $\times$

267   conductivity relationship differed between days (F = 83, $p<0.001$), with the slope becoming

268   more negative from D1 (x = -0.008, $p<0.001$, $r^2 = 0.19$) to D6 (x = -0.07, $p<0.001$, $r^2 = 0.34$),

269   and the estimated marginal mean increased from 3.7 dpm l^{-1} (D1, D2) to 4.1 dpm l^{-1} (Fig. 2).

270   Solving Eq. 4 for the daily [222]Rn and Q fluctuations indicated that groundwater contributions

271   to surface water increased from 35 $\pm$ 30 % on D1 to 61 $\pm$ 50 % on D8 (Table 3).

272   Temperature in HZ (22°C) did not differ significantly from SW, nor between night

273   and day (Table 1). The δ^{18}O-H_2O values differed between surface and subsurface waters (F =

274   4, $p<0.05$). Subsurface $\delta^{18}O$-H_2O values decreased over time (F = 3.3, $p<0.01$), particularly

275   along the north bank, where values tended to be most negative (location: F = 7.8, $p<0.05$;

276   date $\times$ location: F = 3.4, $p = 0.06$) (Table 2). Conductivity was greater in *HZ* than *SW* (F =

277   300, $p<0.001$; Table 2). *HZ* conductivity increased over time (680 ± 50 µS cm^{-1} to 1,200 µS

278   cm^{-1}; F = 160, $p<0.001$), particularly along the north bank (F = 9.3, $p<0.05$; date $\times$ location:

279   F = 30, $p<0.001$). Mass balances based on *HZ* and *SW* conductivity (Eq. 3) show surface

280   water contributions to the subsurface decreased from 83 % on D1 to 62 % on D8 (Table 3).

281

282   3.2 Biogenic gasses (O_2, CO_2, N_2O)

283   Surface water O_2 concentrations varied diurnally from 1.6 ± 0.2 mg l^{-1} (20%

284   saturation) to 1.4 ± 0.2 mg l^{-1} (15% saturation) ($p<0.001$), and decreased from 1.5 ± 0.4 on

285   D1 to 1.4 ± 0.1 mg O_2 l^{-1} on D8 ($p<0.001$; Fig. 2). Best-fit metabolism models accounted for

286   between 60% (D4) and 90% (D6) of diurnal O_2 fluctuations (Suppl. Mat. Fig. S1). Model

287   estimated GPP was 1.3 (0.7 – 3) g O_2 m^{-2} d^{-1} and ER was -28 (-60 - -3) g O_2 m^{-2} d^{-1},

288   producing a GPP/ER ratio of 0.08 (0.03 – 0.1) over the study period (Table 3).

289   Daily dissolved CO_2 negatively correlated with O_2 fluctuations ($r = -0.36$, $p<0.001$;

290   Fig. 2). Over time CO_2 increased from 3.1 ± 0.06 mg C l^{-1} to 3.2 ± 0.03 mg C l^{-1} ($p<0.001$;

291   Fig. 2) and the CH_4:CO_2 concentration ratio decreased from 0.013 to 0.0088 ($p<0.001$;

292   Suppl. Mat Fig. S2). Daily N_2O fluctuations negatively correlated with h ($r = -0.79$,

293     $p<0.001$), ^{222}Rn ($r = -0.067$, $p<0.05$), and O_2 ($r = -0.39$, $p<0.001$), and positively correlated

294   with conductivity ($r = 0.89$, $p<0.001$). Concentrations increased over time from 1.4 µg N_2O-

295   N l^{-1} on D1 to 2.6 µg N_2O-N l^{-1} on D8 ($p<0.001$; Fig. 2), as did estimated marginal means

296   relative to conductivity (690 ± 2 % saturation on D2, 930 ± 3 % saturation on D8). The

297   relationship between N_2O and O_2 saturations changed over time (F = 280, $p<0.001$) from

298   negative on D1 and D2 ($r = -0.6$) to positive on D4 – D8 ($r = 0.1$).

299

3.3 Stream nutrients

Nutrient (DOC, PO_4^{3-}, NO_3^-, NH_4^+) concentrations did not differ significantly

between 'low O_2' and 'high O_2' sampling points in either the *SW*, *S,* or *HZ* samples. Data are

therefore presented as the daily mean for each 24 h period. Surface waters NO_3^-

concentrations increased over time (Suppl. Mat. Table S8), while DOC, and NH_4^+

concentrations decreased (Table 2). Nitrate was 50% of *SW* inorganic N on D1 v. 80% on D8.

Nitrate concentrations tended to be highest along the south bank, both in absolute terms and

relative to conductivity (Table 2). Ammonium tended to be highest along the north bank and

towards the top of the reach (Fig. 3). Nitrate was always higher in *SW* than

Surface sediment (*S*) NO_3^- concentrations decreased from 0.62 mg N l^{-1} on D1 to 0.39

mg N l^{-1} on D8 (F = 6.6, *p*<0.05), while *S* NH_4^+ concentrations remained relatively consistent

over time (Fig. 3; Suppl. Mat. Table S8). This zone had the highest NH_4^+ concentrations (*S* >

HZ > *SW*) and lowest NO_3^- concentrations (*S* < *HZ* < *SW*) (Fig. 3). Spatially, *S* NH_4^+ was

highest in the centre, while NO_3^- increased from the north bank (0.34 ± 0.3 mg N l^{-1}) to centre

(0.39 ± 0.3 mg N l^{-1}) to south bank (0.57 ± 0.4 mg N l^{-1}) (F = 4.0, *p*<0.05; Fig. 3).

Deeper sediment (*HZ*) NO_3^- concentrations increased over time along the south bank

and downstream, while NH_4^+ increased upstream along the north bank (Fig. 3). Over time

NO_3^-:conductivity ratios and DOC concentrations increased at all *HZ* sites (Table 2).

Ammonium concentrations were highest along the north bank (2.3 ± 2 mg N l^{-1}), where NO_3^-

concentrations were lowest (0.12 ± 0.2 mg N l^{-1}). The *HZ* NO_3^- concentrations were lower

upstream (0.48 ± 0.5 mg N l^{-1}) than downstream (1.1 ± 0.8 mg N l^{-1}) (*p*<0.01, Fig. 3), while

DOC concentrations were highest along the north bank (Table 2).

322

3.4. Isotopic composition of inorganic N species

324   3.4.1 Nitrate (δ^{18}O, δ^{15}N)

325   Nitrate isotopes did not differ significantly night v day / high v low tide in either *SW,*

326   *S*, or *HZ*, so data is presented as the mean for each 24 h period. The δ^{15}N-NO$_3^-$ and δ^{18}O-NO$_3^-$

327   values varied significantly over the reach width in *S* and *HZ* (not SW), but did not vary over

328   reach length at any depth (Suppl. Mat. Table S8). δ^{15}N-NO$_3^-$ and δ^{18}O-NO$_3^-$ had distinct

329   patterns over time (Fig. 4). On D1 near-bank δ^{15}N-NO$_3^-$ was +7 ‰ higher in *HZ* than *S*, but

330   this reversed on D4 – D8 with values 0.6 ‰ higher in *S* than *HZ* (Fig. 4). In contrast, *S* δ^{18}O-

331   NO$_3^-$ values were consistently higher than both *SW* and *HZ* (Fig. 4). Over time *S* δ^{18}O-NO$_3^-$

332   increased, especially along the north bank (F = 8.6, *p*<0.01), so the difference between *S* and

333   *SW* δ^{18}O-NO$_3^-$ went from 9.8 ‰ (D1, D2) to 11 ‰ (D6, D8) (Fig. 5).

334   Surface water NO$_3^-$ concentrations correlated with δ^{15}N-NO$_3$- (*r* = 0.63, *p*<0.001), but

335   not δ^{18}O-NO$_3^-$. Over time *SW* δ^{15}N-NO$_3^-$ increased (12 ± 0.5 ‰ to 13 ± 0.2 ‰) while δ^{18}O-

336   NO$_3^-$ decreased (3.9 ± 3 ‰ to 0.35 ± 2 ‰) (Fig. 4). Surface sediment δ^{18}O-NO$_3^-$ values were

337   highest along the north bank (13 ± 4 ‰) and δ^{15}N-NO$_3^-$ values highest in the centre (16 ± 7

338   ‰). Over time south bank *S* δ^{15}N-NO$_3^-$ increased (7.7 ± 2 ‰ to 20 ± 6 ‰) and δ^{18}O-NO$_3^-$

339   decreased (16 ± 5 ‰ to 10 ± 2 ‰; Fig. 4). In *HZ* the δ^{18}O-NO$_3^-$, but not δ^{15}N-NO$_3^-$, decreased

340   from the north bank (9.2 ± 6 ‰) to centre (4.9 ± 6 ‰) to south bank (4.0 ± 2 ‰). Over time

341   *HZ* δ^{15}N-NO$_3^-$ decreased from 15 ± 10 ‰ on D1 to 13 ± 1 ‰ on D6 (Fig. 5). Accordingly,

342   the linear relationship between δ^{18}O-NO$_3^-$ v δ^{15}N-NO$_3^-$ was never strong, but shifted from

343   weakly negative in *SW* (slope = -0.7, *p*<0.001, r^2 = 0.04) to more clearly negative in *S* (slope

344   = -0.3, *p*<0.001, r^2 = 0.14), to positive in *HZ* (slope = 0.5, *p*<0.001, r^2 = 0.19).

345

346   3.4.2 N$_2$O (δ^{18}O, δ^{15}N, SP)

347   Nitrous oxide isotopes (δ^{18}O, δ^{15}N, and SP), measured at the nine *SW* sampling

348   locations, differed neither between day/night samplings nor between locations (Suppl. Mat.

349   Fig. S3). Over time δ^{15}N-N_2O values decreased from 1.5 ± 2 ‰ to -0.99 ± 0.9 ‰ ($F = 26$,

350      $p<0.001$; Fig. 6). The δ^{18}O-N_2O values were lower on D1 (52 ± 6 ‰) than D2 – D8 (57 ± 4

351   ‰) ($F = 20$, $p<0.001$), while SP increased from 15‰ on D1 to 31‰ on D8 ($F = 200$,

352      $p<0.001$). Changes in δ^{18}O-N_2O related inversely to δ^{15}N-N_2O ($y = 16 - 0.26x$, $p<0.001$, $r^2 =$

353   0.45) and positively to SP ($y = -56 + 1.3x$, $p<0.001$, $r^2 = 0.61$) (Fig. 6). Consequently, the

354   difference between δ^{18}O-N_2O and δ^{18}O-NO_3^- at each site increased over time from 49‰ to

355   58‰ ($F = 15$, $p<0.001$), while δ^{15}N-N_2O decreased relative to the corresponding δ^{15}N-NO_3^-

356   from -10‰ on D1 to -14‰ on D8 ($F = 90$, $p<0.001$).

357

358   **4. Discussion**

359   4.1 Hydrologic setting

360   Tides often dominant daily water chemistry fluctuations at the marine end of estuaries

361   (Call et al., 2015), but were expected to be secondary to internal productivity in this nutrient-

362   rich freshwater zone ~100 km inland (Knights et al., 2017). The distinctly tidal fluctuations in

363   depth, v and conductivity (Fig. 2) are likely made more apparent due turbidity masking any

364   diurnal metabolism. The fact that daily ^{222}Rn fluctuated with v and h also suggests the tidal

365   shifts in hydraulic pressure could be 'pumping' the subsurface and influence hyporheic

366   exchange (Barnes et al., 2019; Bianchin et al., 2011). However, these daily fluctuations are

367   overprinted by continuous declines in h and Q (Fig. 2, Table 2). Decreasing Q, which could

368   promote internal N reactions over downstream discharge (Ocampo et al., 2006; Raymond et

369   al., 2016; Wollheim et al., 2018), is clear. Yet the h and v shifts could also alter microbial N

370   transformations vis-à-vis subsurface exchange (Hester et al., 2019; Krause et al., 2017;

371   Lewandowski et al., 2019; Singh et al., 2019).

372   Multiple lines of evidence suggest that the connection between surface water and

373   groundwater changed over the study period. The increased surface water ^{222}Rn (Table 3) fits

374 expectations that groundwater inputs decrease during high flow events and then increase as

375 the system returns to baseflow (Looman et al., 2016; Schubert and Paschke, 2015; Webb et

376 al., 2017). However, this is complicated by the concurrent dampening tidal ^{222}Rn fluctuations,

377 which suggest weakening tide-driven pumping, and thus vertical mixing (Call et al., 2015).

378 Decreased vertical mixing during the return to baseflow conditions is supported by, first, the

379 growing spatial variability in subsurface δ^{18}O-H$_2$O, as incomplete mixing is needed for

380 isotopically distinct pools to develop (Dudley-Southern and Binley, 2015), and, second,

381 increased difference between surface and subsurface conductivities (Table 3). Thus falling v

382 and h led to both more groundwater dominated surface waters and dampened vertical

383 exchange within the channel. This provides a strong framework for empirically evaluating

384 hydrologic regulations of stream NO$_3^-$ and N$_2$O processing.

385

386 4.2 Biological setting (metabolism)

387   Diurnal light variations that shift streams from net respiration (O$_2$ consuming) at night

388 to net photosynthesis (O$_2$ producing) during the day (Bernhardt et al., 2018; Parker et al.,

389 2005) can impact N cycling (Martí et al., 2020; Yang et al., 2019). Previous work shows that

390 NO$_3^-$ concentrations similar to those measured here can fuel biological growth to the extent

391 that O$_2$ fluctuates >100% between night and day (Clough et al., 2007; Harrison et al., 2005).

392 Yet despite the warm temperatures and high nutrient concentrations, daily O$_2$ varied by only

393 5% (Fig. 2). Notably, unlike other systems where muted diurnal O$_2$ signals reflected low

394 biological activity (e.g., Baulch et al., 2012), here the low O$_2$ (~ 20% saturation) and high

395 CH$_4$:CO$_2$ ratios instead indicate strong heterotrophy (Stanley et al., 2016). This fits with

396 metabolism model estimates that reach respiration was 5 – 20 times higher than productivity

397 (Table 3). A strongly heterotrophic system is reasonable given the observed low water clarity

398 that would inhibit photoautotrophic activity (see photos in Fig. 1, Fig. 7) and high nutrient

399   loads to fuel respiration. This contradicts the expectation that increased nutrients + light fuel

400   plant growth in highly impacted waterways (Tank et al., 2010). However, we observed a

401   similar turbidity-driven productivity drop in other highly modified subtropical waterways

402   (Wells and Eyre, 2019; Wells et al., 2020). The markedly low productivity here thus provides

403   a critical contrast to previous metabolism × N investigations, which found light fluctuations

404   drove N uptake vis-à-vis primary productivity (Fork and Heffernan, 2014; Hall and Tank,

405   2003; Reisinger et al., 2019). For our purposes the key implications of the apparently light-

406   limited metabolic regimen are that, 1) assimilatory phototrophic N demand will be minimal,

407   and, 2) low O_2 and high C create favourable denitrification conditions.

408

409   4.3 Nitrate

410   The increasing surface water NO_3^- concentrations over time contradict the hypothesis

411   that Q regulates solute export by decreasing in-stream processing (Alexander et al., 2009;

412   Raymond et al., 2016; Wollheim et al., 2018). Downstream NO_3^- export actually increased

413   from 250 to 410 kg N d^{-1} despite Q decreasing by 30% (Fig. 7). Similar NO_3^- increases

414   following hydrologic 'pulses' were previously observed (Chen et al., 2020; McKee et al.,

415   2000; Ocampo et al., 2006), but it is unclear whether this is due to either new NO_3^- sources

416   entering the system or changing internal N cycling.

417

418   4.3.1. Hydrologic NO_3^- sources

419   Increased solute export following high-flow events can come from either overland

420   flow or increased groundwater inputs (Ocampo et al., 2006; Webb et al., 2017). A new

421   upstream source emerging during this study's narrow sampling window can be reasonably

422   ruled out due to the magnitude of the established WWTP source and lack of branching

423   tributaries (Fig. 1). However, infiltration of shallow, N-rich groundwater (Table 1) could

424 affect surface water NO_3^-. Significant groundwater NO_3^- inputs aligns with evidence that

425 groundwaters comprised a greater proportion of stream flow over time (Table 3), and is

426 supported by the spatial distribution of streambed N. The highest sediment N concentrations

427 cluster along the north bank near the groundwater plume (Fig. 1, Fig. 3) and NO_3^- depth

428 profiles are inverted relative to what is created when surface water is the sole NO_3^- source

429 (Kessler et al., 2013; Schutte et al., 2015). However, the significance of groundwater N to the

430 measured surface water concentrations would depend on the extent of denitrification during

431 transport through the sediments (Trauth and Fleckenstein, 2017; Trauth et al., 2014). Changes

432 in NO_3^- isotopic composition constrain this factor: conservative groundwater-to-surface water

433 transport (no sediment denitrification) would cause SW NO_3^- to become isotopically similar

434 HZ NO_3^- as the groundwater contribution increased, while reactive transport (incomplete

435 sediment denitrification) would fractionate upwelling NO_3^- and cause SW NO_3^- to become

436 isotopically heavier than HZ NO_3^- (Wells et al., 2019). Neither scenario is reflected in the

437 relatively low SW $\delta^{15}N$-NO_3^- and $\delta^{18}O$-NO_3^- values that persisted throughout the study (Fig.

438 5). Instead, the increasing isotopic depletion, rather than enrichment or equivalence, of SW

439 NO_3^- relative to subsurface NO_3^- shows that the net increase in upwelling groundwater was

440 not the main driver of increasing surface water NO_3^-. This indicates that changing within-

441 stream cycling, rather than external inputs, regulated NO_3^- concentrations.

442

443 4.3.2. Biological NO_3^- cycling

444   Relatively warm water temperatures and high substrate concentrations would provide

445 ample 'capacity' for a range of N transformations within the sampled reach. However, the

446 apparently light-limited stream productivity also negated the photoautotrophic nutrient

447 demand, which would cause diel surface water NO_3^- concentration fluctuations (Appling and

448 Heffernan, 2014; Chamberlin et al., 2019; Cohen et al., 2012). This finding is important as it

449 suggests that dissimilatory microbial pathways, rather than assimilation and mineralisation by

450 algae and plants, are the likely drivers of stream N dynamics.

451   Increasing surface water NO_3^- export could come from either decreased removal

452 (denitrification) or increased production (nitrification). The changed flow dynamics and

453 hyporheic exchange would affect the opportunity for both to occur (Azizian et al., 2017;

454 Briggs et al., 2014; Harvey et al., 2013; Naranjo et al., 2015). Denitrification can be limited

455 under high flows when there is insufficient time for anoxic zones to form (Kessler et al.,

456 2013; Zarnetske et al., 2012). Nitrification is maximised under 'intermediate' flows that limit

457 the extent of anoxic sites (Azizian et al., 2017; Zarnetske et al., 2012). Declining hyporheic

458 exchange, which regulates stream denitrification by transporting NO_3^- to denitrifying zones

459 (Gomez-Velez et al., 2015), could also shift the nitrification-denitrification balance.

460   Nitrate isotopes help tease apart the relative importance of decreasing denitrification v

461 increasing nitrification on surface water NO_3^- fluxes. First, denitrification causes a

462 characteristic parallel enrichment in $\delta^{15}N\text{-}NO_3^-$ v $\delta^{18}O\text{-}NO_3^-$ (Granger and Wankel, 2016;

463 Wells et al., 2019), which was not evident here (Fig. 4). Second, nitrification can be

464 constrained based on $\delta^{18}O\text{-}NO_3^-$ values because nitrifiers incorporate O from the surrounding

465 water and dissolved O_2. Assuming these are incorporated at a ratio of $2\times O\text{-}H_2O$ to $1 \times O\text{-}O_2$

466 (Kendall, 1998), and using measured $\delta^{18}O\text{-}H_2O$ values and 23.5‰ for $\delta^{18}O\text{-}O_2$ (Kroopnick

467 and Craig, 1972), here nitrification-produced $\delta^{18}O\text{-}NO_3^-$ values would be ~5‰ (Fig. 5).

468 However, this common parameterisation likely over-estimates $\delta^{18}O\text{-}NO_3^-$ as it does not

469 account for fractionation during incorporation or exchange with surrounding H_2O (Buchwald

470 et al., 2012). Thus any within-stream nitrification here likely produced $\delta^{18}O\text{-}NO_3^-$ values

471 between -10‰ (Fang et al., 2012) and -4‰ (Boshers et al., 2019). Although admittedly

472 broad, surface water $\delta^{18}O\text{-}NO_3^-$ clearly shifted to this 'nitrification' range over time while

473   sediment $\delta^{18}O$-NO_3^- values remained relatively enriched (Fig. 5). In-situ production, rather

474   than decreased removal, thus likely increased surface water NO_3^- export over time.

475   Increasing nitrification as hyporheic exchange declined is reasonable in this setting.

476   First, the low light conditions would favour nitrification. Aquatic nitrification is generally

477   highest when turbidity or depth inhibit phytoplankton growth, removing competition for any

478   available NH_4^+ (Smith et al., 2014; Stephens et al., 2019; Xu et al., 2019). Second, stream

479   sediments would provide an ample NH_4^+ supply to the overlying water (Fig. 3), regardless of

480   the potential ~10% bias associated with the S DET probes (Briggs et al., 2015; Comer-

481   Warner et al., 2020a). While very high, the porewater concentrations fit within the ~30 – 100

482   mg NH_4^+-N l^{-1} range of other sewage-impacted (Gupta and Karuppiah, 1996; Palmer-Felgate

483   et al., 2010) and hypereutrophic (Morgan et al., 2012) systems. We therefore proposed that

484   decreased hyporheic mixing increased NO_3^- release into the surface water (net nitrification)

485   by minimising transport between oxic (NO_3^- rich) and anoxic (denitrifying) microsites in the

486   subsurface (Harvey et al., 2013; Kessler et al., 2013).

487

488   4.4 Surface water N_2O cycling

489   Increasing N_2O emissions could result from decreased reduction or increased

490   production via either denitrifying or nitrifying pathways. However, like NO_3^- export, stream

491   N_2O emissions are often assumed to be regulated by denitrification (Beaulieu et al., 2011;

492   Hampton et al., 2020). This is partially based on inverse O_2:N_2O relationships observed

493   between days, seasons, and systems (Ji et al., 2018; Laursen and Seitzinger, 2004; Rosamond

494   et al., 2012; Venkiteswaran et al., 2014). Here a similar negative O_2:N_2O relationship was

495   found on the first two sampling dates (Fig. 2). This relationship could reflect stream biology,

496   with sediment oxygenation at high tide inhibiting denitrification (Barnes et al., 2019; Knights

497   et al., 2017)). Alternatively, tidal flushing of N_2O rich, O_2 poor porewaters at low tide would

498   produce the same pattern (Reading et al., 2017). It then follows that the shift towards a

499   positive $O_2:N_2O$ relationship that emerged on the subsequent three sampling dates (Fig. 2)

500   was due to either a shift away from denitrification-driven (O_2-limited) N_2O production or

501   tidal flushing decreasing along with hyporheic exchange.

502   The N_2O isotope data confirmed that in-stream biological production changed over

503   time as N_2O emissions increased (Fig. 6, Fig. 7). Increasingly negative $\delta^{15}N$-N_2O values over

504   time could be caused by either increasing nitrification (^{15}N enrichment factor, $^{15}\varepsilon$, of -56‰

505   for $NH_2OH \rightarrow N_2O$) relative to bacterial denitrification ($^{15}\varepsilon = -20$‰ for $NO_2^- \rightarrow N_2O$) or a

506   decline in N_2O reduction to N_2, which progressively enriches the residual N_2O pool ($^{15}\varepsilon = -6$

507     $- 7$ ‰) (Denk et al., 2017; Lewicka-Szczebak et al., 2017). Yet here the simultaneous

508   increases in SP and $\delta^{18}O$-N_2O clearly confirm that increased N_2O over time was produced by

509   net nitrification increasing, not denitrification or N_2O reduction (Fig. 5). This is because, 1)

510   nitrification produces N_2O with higher SP (~30, (Frame and Casciotti, 2010)) than microbial

511   denitrification (SP ~0, (Haslun et al., 2018)), 2) the SP v. $\delta^{18}O$-N_2O slope of ~2 is greater

512   than the ~0.5 produced by N_2O reduction (Lewicka-Szczebak et al., 2017), and, 3) the

513   inverse, rather than parallel, relationship between $\delta^{15}N$-N_2O and $\delta^{18}O$-N_2O rules out N_2O

514   reduction (Snider et al., 2013). Denitrification (or flushing N_2O from denitrifying sediment

515   zones) controlled surface water N_2O when Q and hyporheic exchange were high, but as water

516   levels dropped nitrification became the dominant N_2O source. The importance of nitrification

517   was surprising given the high C, low O_2, and high NO_3^- conditions, but adds to similar

518   findings from a hypoxic lake (Salk et al., 2016) to suggest that nitrification-driven N_2O

519   emissions may be more widespread in low O_2 aquatic systems than previously assumed.

520

521   4.5 Implications for understanding stream N_2O emissions

522 Nitrous oxide emissions from the sampled reach were relatively high. Yet the

523 calculated fluxes were between ~ 200% to <50% of those reported from streams with

524 comparable surface water NO_3^- concentrations (Clough et al., 2007; Harrison and Matson,

525 2003; McMahon and Dennehy, 1999). Notably, the two sites with relatively low N_2O

526 emissions (Clough et al., 2007; Harrison and Matson, 2003) had strong diurnal O_2 and N_2O

527 fluctuations. Turbid and low O_2 waterways like Monaltrie Creek are ubiquitous across the

528 global tropics (Julian et al., 2013) and the Australian continent (Bormans et al., 2004; Oliver

529 et al., 2010). Yet surveying the literature collated here indicates that scientific understanding

530 of stream N_2O (and N) dynamics is primarily based on clear, temperate, northern hemisphere

531 streams < 1 m deep. The role of photoautotrophic N substrate competition in regulating N_2O

532 emissions should be more carefully constrained.

533 The data here provides direct confirmation of the hypothesis that stream hydrology

534 (opportunity) controls biogenic N_2O emissions (Marzadri et al., 2017; Quick et al., 2016).

535 While many models have been used to assess how flow fluctuations affect stream N cycling

536 (e.g., Azizian et al., 2017; Hester et al., 2019; Rahimi et al., 2015), this study provides one of

537 the first in-situ validations of these interactions. However, while we confirmed that lower

538 flows can make stream reaches become more 'transforming' and less 'transporting'

539 (O'Donnell and Hotchkiss, 2019), we found this shift enhanced NO_3^- and N_2O production

540 rather than removal. Such nitrification-driven N_2O and NO_3^- fluxes has implications for

541 aquatic N_2O modelling: it suggests that the frequently observed positive correlations between

542 NO_3^- and N_2O could reflect microbial coproduction during in-stream nitrification rather than

543 an 'emissions factor' of downstream NO_3^- transport (Kroeze et al., 2005).

544

545

546

Research data

Data from loggers (including dissolved gas concentrations) and daily sampling (including
isotope data) are available for download: https://figshare.com/s/d94125b33e7bd6be5bd8 and
https://figshare.com/s/da127a3af8e6c2eeec25. *Note these data links are supplied for
reviewing purposes only. Links will be updated to DOIs once the manuscript is accepted.*

572   **Tables**

573   **Table 1** Summary of water chemistry recorded during routine monitoring of, 1) surface water at the study site, and, 2) eight groundwater wells
574   installed at either shallow (0.05 m) or deep (0.2 m) depths in the unconfined aquifer between the WWTP and the study site (Fig. 1). Values
575   represent the mean (± SD) of samples collected quarterly over the four years prior to the present study.

	DO	Conductivity	DOC	NH_4^+	NO_3^-
	$mg\ l^{-1}$	$\mu S\ cm^{-1}$	$mg\ l^{-1}$	$mg\ N\ l^{-1}$	$mg\ N\ l^{-1}$
Surface water	4.9 (1)	510 (200)	8.4 (5)	0.45 (0.3)	1.4 (1)
Shallow groundwater	2.8 (1)	4,400 (3,000)	17 (10)	0.99 (1)	0.20 (0.4)
Deep groundwater	1.9 (1)	2,700 (1,000)	8.0 (7)	6.7 (6)	0.78 (3)

576

577
578
579
580
581
582
583
584
585
586
587
588
589
590

		Surface water					Hyporheic Zone				
		δ^{18}O-H$_2$O ‰ v. VSMOW	T °C	Cond. µS cm^{-1}	NO$_3^-$:Cond. µg N µS^{-1}	DOC mg l^{-1}	δ^{18}O-H$_2$O [c] ‰ v. VSMOW	T °C	Cond. µS cm^{-1}	NO$_3^-$:Cond. µg N µS^{-1}	DOC mg l^{-1}
D1	North bank	-3.6 (0.06)		270 (30)	3.7 (0.9)	1.0 (0.01)	-3.7 (0.7)	23 (1)	710 (70)	0.52 (0.4)	5.9 (2)
	Centre	-3.7 (0.02)		260 (20)	4.7 (0.5)	0.98 (0.07)	-3.6 (0.6)	22 (0.6)	670 (20)	1.2 (0.7)	3.6 (2)
	South bank	-3.7 (0.02)	21 (0.9)	260 (4)	4.9 (0.2)	0.95 (0.07)	-3.5 (1)	21 (0.1)	670 (20)	1.4 (0.3)	3.3 (2)
D2	North bank	-3.7 (1)		270 (10)	5.8 (0.3)	0.94 (0.1)	-4.2 (0.3)	22 (3)	600 (100)	0.25 (0.3)	3.6 (1)
	Centre	-3.7 (0.7)		270 (10)	6.0 (0.3)	0.95 (0.2)	-3.1 (0.9)	23 (0.4)	620 (100)	2.2 (1)	2.2 (0.7)
	South bank	-3.3 (0.8)	21 (0.3)	280 (6)	6.3 (0.3)	0.89 (0.1)	-3.6 (0.5)	23 (0.4)	600 (70)	2.5 (0.6)	2.0 (1)
D4	North bank	-3.8 (0.5)		300 (20)	5.5 (0.5)	0.75 (0.08)	-4.3 (1)	21 (2)	680 (100)	0.08 (0.1)	3.1 (0.7)
	Centre	-3.6 (0.4)	22 (0.3)	290 (20)	5.6 (0.4)	0.77 (0.05)	-3.8 (0.4)	21 (2)	650 (60)	1.7 (1)	2.0 (0.3)
	South bank	-3.9 (0.3)		280 (60)	7.0 (3)	0.77 (0.02)	-3.9 (0.9)	21 (2)	620 (60)	2.6 (0.7)	2.1 (0.9)
D6	North bank	-4.8 (0.5)		300 (9)	6.4 (0.4)	0.78 (0.08)	-5.6 (0.6)	23 (0.9)	1,100 (200)	0.05 (0.03)	9.5 (5)
	Centre	-4.4 (1)	21 (0.5)	290 (7)	6.4 (0.3)	0.75 (0.03)	-4.9 (0.5)	23 (2)	930 (50)	1.4 (0.9)	2.9 (1)
	South bank	-5.0 (0.7)		300 (10)	6.5 (0.2)	0.75 (0.05)	-4.1 (1)	23 (0.4)	910 (20)	1.7 (0.4)	2.7 (1)
D8	North bank	-4.8 (1)		350 (6)	7.1 (0.2)	0.73 (0.05)	-4.4 (0.7)	22 (0.9)	1,700 (200)	0.02 (0.02)	8.9 (2)
	Centre	-4.8 (2)	21 (0.6)	350 (8)	7.1 (0.2)	0.71 (0.05)	-3.9 (1)	22 (0.7)	1,000 (200)	1.5 (1)	3.5 (2)
	South bank	-4.6 (0.8)		350 (4)	7.1 (0.1)	0.72 (0.05)	-3.0 (2)	22 (1)	1,000 (200)	1.8 (1)	3.5 (3)

595 *Samples were targeted at night v day (D1 – D4) and low v high tides (D6 – D8)

596

597 **Table 3:** Summary of stream metabolism (productivity / respiration ratio, P/R), the fractional contribution to groundwater to surface water (f_{GW}),
598 and fractional contribution of surface water back into the hyporheic zone (f_{sw}). The P/R ratio was modelled based on surface water O_2
599 concentrations measured in the centre of the reach (see Suppl. Mat. 2). Values of f_{GW} were calculated using surface water ^{222}Rn concentrations
600 logged in the reach centre, and f_{sw} by comparing conductivity measured twice per sampling date at nine locations in the surface water and 20 cm
601 below the sediment surface (*HZ*) to that of local groundwater, where uncertainty ranges are based on maximum and minimum end-member
602 values (see Suppl. Mat. 3).

603

Date	P/R	f_{GW}	f_{sw}
D1	0.05	0.35 (0.05 – 0.65)	0.83 (0.73 – 0.87)
D2	0.2	0.32 (0.02 – 0.62)	0.86 (0.75 – 0.92)
D4	0.1	0.54 (0.14 – 0.94)	0.86 (0.75 – 0.91)
D6	0.005	0.58 (0.08 – 1.1)	0.72 (0.51 – 0.82)
D8	0.03	0.61 (0.11 – 1.1)	0.62 (0.24 – 0.82)

604

Figure captions

606 **Fig. 1** Samples were collected from Monaltrie Creek (b), a tributary of the Wilson River near

607 Lismore, NSW (a). The sampled reach (red box) is downstream of a wastewater treatment

608 plant (WWTP) that discharges inorganic N (DIN) into the surface and groundwater. Samples

609 were collected from the surface water (*SW*), surface sediments (*S*), and deeper hyporheic

610 zone (*HZ*) from the north bank, centre, and south bank of the channel at three locations (b).

611 Shading in (a) represents mean NH_4^+ + NO_3^- concentrations measured during routine

612 monitoring of the shallow groundwater (black triangles) and creek (circles) the year prior to

613 the study; the arrow indicates the groundwater flow direction.

614

615 **Fig. 2** Changes in surface water conditions over eight days in a highly eutrophic stream in

616 sub-tropical NSW, Australia: (a) stream height and flow velocity, *v*; (b) ^{222}Rn and

617 conductivity; (c) dissolved O_2 (DO) and CO_2; (d) N_2O and NO_3^- concentrations. Parameters

618 were measured over five diurnal cycles (D1, D2, D4, D6, D8). Stream height, *v*, and ^{222}Rn

619 were recorded every 5 min, CO_2 and N_2O every 1 sec, and DO every 15 min. Nitrate

620 concentrations were measured in samples collected from nine locations across the reach twice

621 every 24 h. Gaussian smoothing (black lines) was applied to the *v* and ^{222}Rn data (black

622 points; a, b). Dashed red lines indicate water sampling times.

623

624 **Fig. 3** Changes the NH_4^+ (a, b, c) and NO_3^- (d, e, f) concentrations of the surface water (*SW*),

625 top 5 cm of the sediments (*S*), and hyporheic zone (*HZ*; 30 cm below the sediment surface)

626 on over an eight-day sampling period (D1 - D8) in a stream reach during falling discharge

627 conditions. Samples were collected from near the north bank, centre, and south bank of the

628 stream at three locations along the reach (water flows A → C). Shaded areas are interpolated

629 between sampling points (black circles; *n* = 2). Note different scale for *S* NH_4^+ concentrations

630 (*), and the exaggerated vertical scale. See Suppl. Mat. Tables S5 – S7 for D2 and D6 data

631 and Suppl. Mat Table S8 for outputs from statistical tests.

632

633 **Fig. 4** The NO_3^- isotopic composition ($\delta^{15}N$-NO_3^- v. $\delta^{18}O$-NO_3^-) in the surface water (*SW*: a,

634 b, c), surface sediments (*S*: d, e, f) and hyporheic zone (*HZ*: g, h, i) of a subtropical stream

635 over eight days of falling water levels (from D1, black circles, to D8, light grey circles).

636 Samples were collected near the north bank (a, d, g), centre (b, e, h), and south bank (c, f, i).

637 Points represent the mean ($\pm$ SD) of samples from three locations along the length of the 30

638 m reach, which were collected twice over each 24 h period ($n = 6$). Coloured rectangles show

639 the mean $\pm$ SD range for the whole sampling period. Mixed model analysis (F and *p* values)

640 for $\delta^{18}O$-NO_3^- and $\delta^{15}N$-NO_3^- variations over the stream width and time are shown.

641

642 **Fig. 5** The $\delta^{15}N$-NO_3^- (a), $\delta^{18}O$-NO_3^- (b), and NO_3^- concentrations (c) at 5 cm and 20 cm

643 depth in the sediments (brown) and in the surface water (blue), as measured during high flow

644 conditions (D1) and then eight days later after water levels fell (D8). Dashed lines in (b)

645 indicate the theoretical $\delta^{18}O$-NO_3^- composition produced from in-situ nitrification (S1:

646 mixing $2\times O$-H_2O and $1\times O$-O_2; S2: mixing + kinetic fractionation; outputs from S3, mixing +

647 kinetic fractionation + exchange fell below the scale of the plot). Surface water N_2O

648 concentrations (mean $\pm$ SD over three hours around each sampling point) are also shown (c).

649

650 **Fig. 6** The isotopic composition of surface water N_2O, measured five times over eight days as

651 stream flow declined (D1 $\rightarrow$ D8). Each $\delta^{15}N$-N_2O, $\delta^{18}O$-N_2O and ^{15}N site preference (SP)

652 value represent the mean $\pm$ SD of samples collected at nine locations across the width and

653 length of a stream reach; measurements were carried out twice during each 24-hr period. The

654 $\delta^{18}O$-N_2O values are corrected for mixing with atmospheric N_2O (Eq. 1); crosses represent

655   uncorrected values. Solid lines represent the best-fit of the linear regression between δ^{18}O-

656   N_2O and SP (a; y = -56 + 1.3x, $p<0.001$, $r^2 = 0.61$) and δ^{15}N-N_2O and δ^{18}O-N_2O (b; y = 16 –

657   0.26x, $p<0.001$, $r^2 = 0.45$), with grey shading over the 95% CI. Dashed lines indicate the SP

658   v δ^{18}O-N_2O (a) and δ^{15}N-N_2O v δ^{18}O-N_2O (b) relationships produced during N_2O reduction

659   to N_2 (Lewicka-Szczebak et al., 2017; Ostrom et al., 2007). The mean surface water N_2O

660   saturation for the three hours around each sampling point is shown (blue points and line).

661

662   **Fig. 7** Over eight days the surface water depth and discharge (*Q*) decreased, causing surface

663   waters to become more groundwater (yellow) dominated as it returned toward baseflow, and

664   less surface water (brown) reached the hyporheic sediment zone (orange). The combination

665   of decreased exchange and increased residence time enhanced biological oxidation of the

666   large sediment NH_4^+ pool, increasing water-air N_2O emissions and downstream NO_3^-

667   discharge. Photos are from two days prior to D1 (left) and on D6 (right), credit: N.S. Wells.

668

669

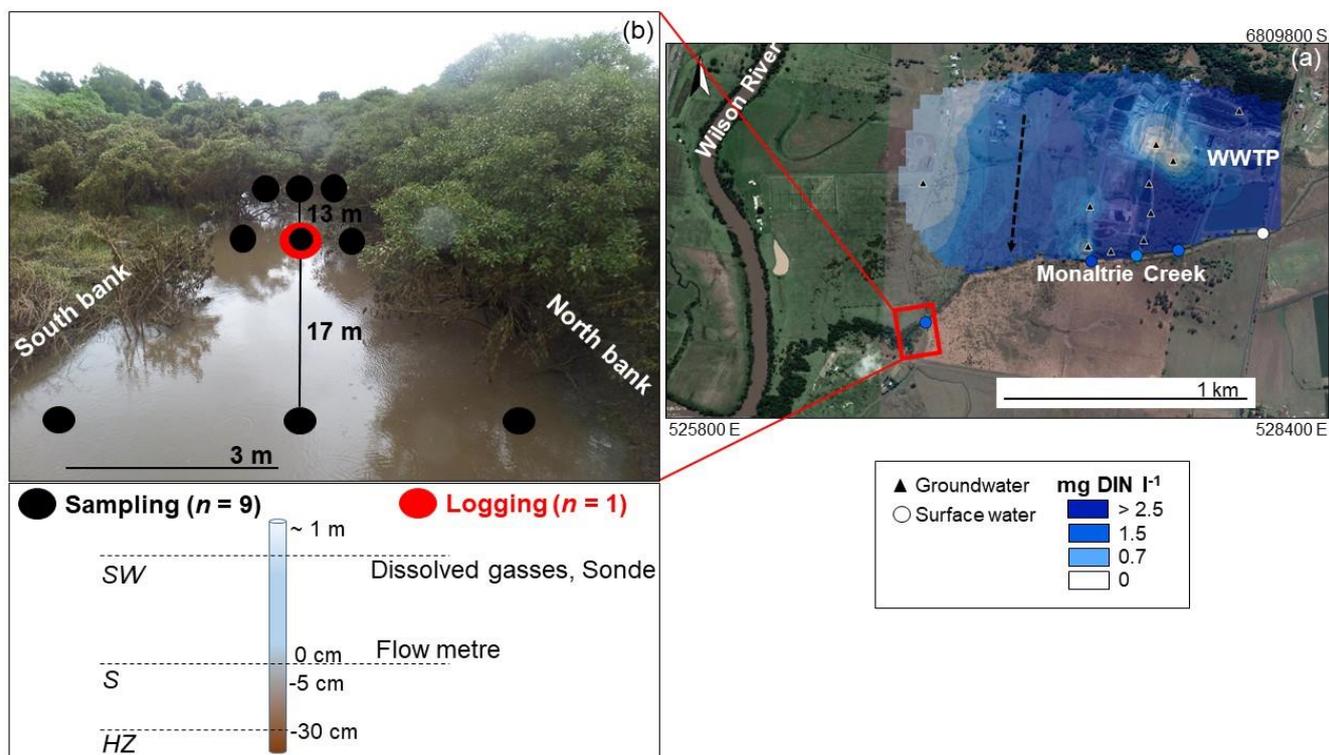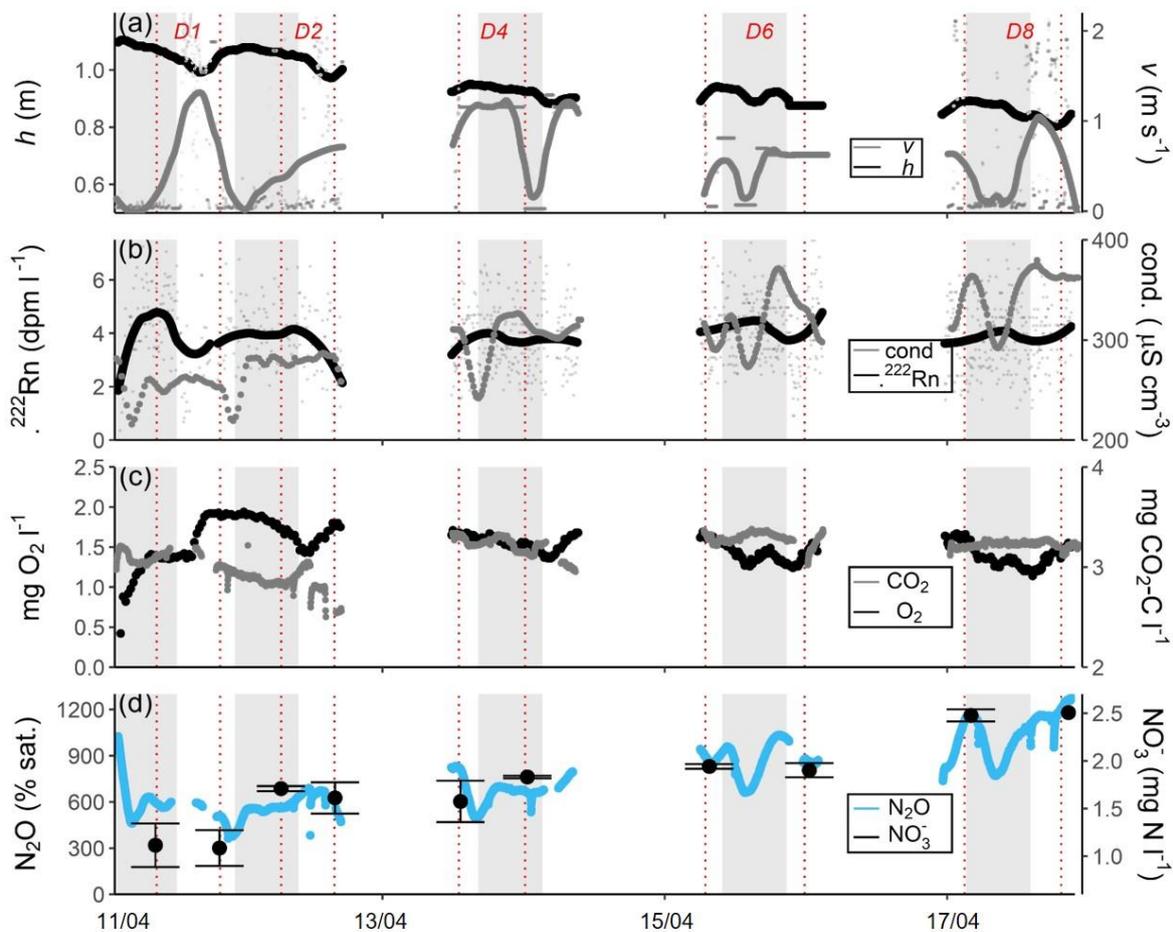670

671

672

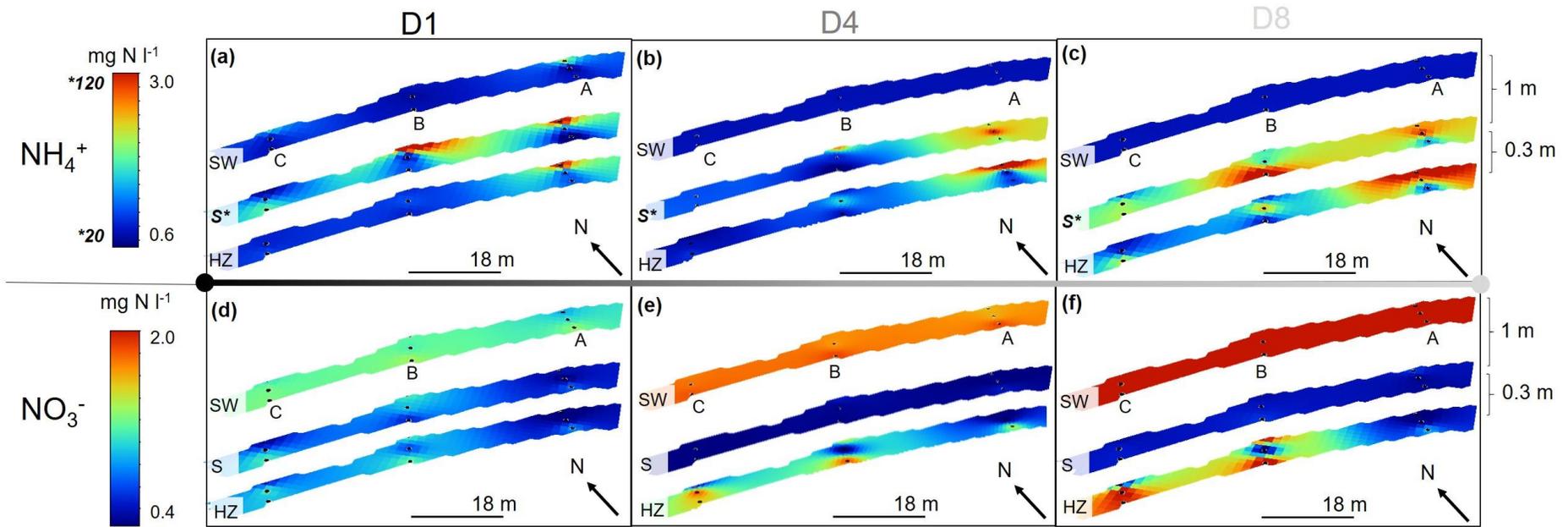673

674

675

676

677

678

679

Figures

Figure 1:

Fig. 1 Samples were collected from Monaltrie Creek (b), a tributary of the Wilson River near

Lismore, NSW (a). The sampled reach (red box) is downstream of a wastewater treatment

plant (WWTP) that discharges inorganic N (DIN) into the surface and groundwater. Samples

were collected from the surface water (*SW*), surface sediments (*S*), and deeper hyporheic

zone (*HZ*) from the north bank, centre, and south bank of the channel at three locations (b).

Shading in (a) represents mean $NH_4^+ + NO_3^-$ concentrations measured during routine

monitoring of the shallow groundwater (black triangles) and creek (circles) the year prior to

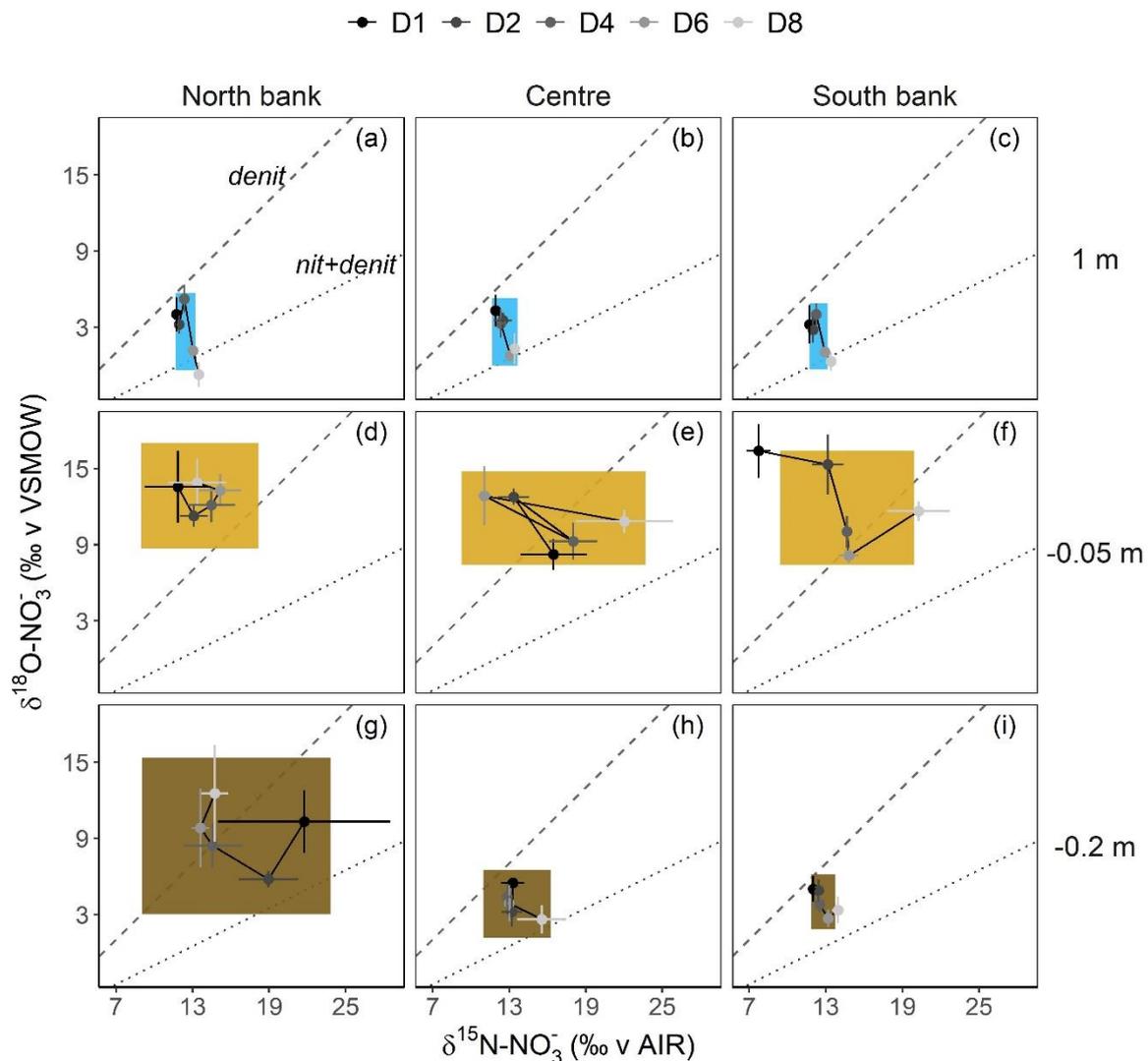the study; the arrow indicates the groundwater flow direction.

Figure 2

696

Fig. 2 Changes in surface water conditions over eight days in a highly eutrophic stream in
sub-tropical NSW, Australia: (a) stream height and flow velocity, *v*; (b) ^{222}Rn and
conductivity; (c) dissolved O_2 (DO) and CO_2; (d) N_2O and NO_3^- concentrations. Parameters
were measured over five diurnal cycles (D1, D2, D4, D6, D8). Stream height, *v*, and ^{222}Rn
were recorded every 5 min, CO_2 and N_2O every 1 sec, and DO every 15 min. Nitrate
concentrations were measured in samples collected from nine locations across the reach twice
every 24 h. Gaussian smoothing (black lines) was applied to the *v* and ^{222}Rn data (black
points; a, b). Dashed red lines indicate water sampling times.

Fig. 3 Changes in NH_4^+ (a, b, c) and NO_3^- (d, e, f) concentrations of the surface water (*SW*), top 5 cm of the sediments (*S*), and hyporheic zone

(*HZ*; 30 cm below the sediment surface) on over an eight-day sampling period (D1 - D8) in a stream reach during falling discharge conditions.

Samples were collected from near the north bank, centre, and south bank of the stream at three locations along the reach (water flows A → C).

Shaded areas are interpolated between sampling points (black circles; $n = 2$). Note the difference in scale for *S* NH_4^+ concentrations (*), and the

exaggerated vertical scale. See Suppl. Mat. Tables S5 – S7 for D2 and D6 data and Suppl. Mat Table S8 for outputs from statistical tests.

Figure 4

Fig. 4 The NO$_3^-$ isotopic composition (δ^{15}N-NO$_3^-$ v. δ^{18}O-NO$_3^-$) in the surface water (1 m: a,

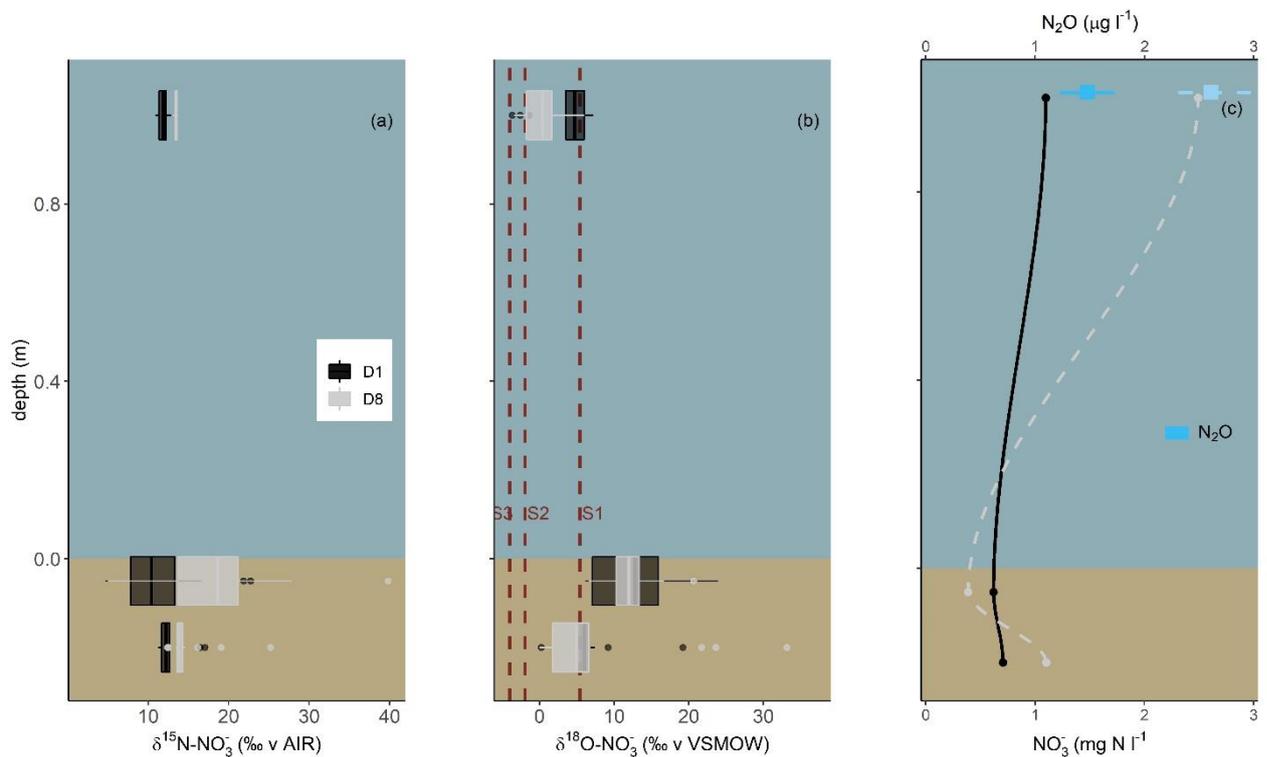b, c), surface sediments (-0.05 m: d, e, f) and hyporheic zone (-0.2 m: g, h, i) of a stream

reach over eight days (D1, black circles, to D8, light grey circles) of falling *Q*. Points

represent the mean (± SE) of samples collected twice over each 24 h period from three

locations along the 30 m reach, which were (*n* = 6) across the width of the stream: along the

north bank closest to the pollution source (a, d, g), centre (b, e, h), and south bank (c, f, i).

Coloured rectangles show the mean ± SD range for the whole sampling period. See Suppl.

Mat Table S8 for associated mixed model results.

723 *Figure 5*

724

Fig. 5 The δ^{15}N-NO$_3^-$ (a), δ^{18}O-NO$_3^-$ (b), and NO$_3^-$ concentrations (c) at 5 cm and 20 cm

depth in the sediments (brown) and in the surface water (blue), as measured during high flow

conditions (D1) and then eight days later after water levels fell (D8). Dashed lines in (b)

indicate theoretical δ^{18}O-NO$_3^-$ composition produced from in-situ nitrification (S1: mixing

$2\times$O-H$_2$O and $1\times$O-O$_2$; S2: mixing + kinetic fractionation; S3: mixing + kinetic fractionation

+ exchange produce δ^{18}O-NO$_3^-$ equal to surrounding δ^{18}O-H$_2$O). Surface water N$_2$O

concentrations (mean ± SD over three hours around each sampling point) are also shown (c).
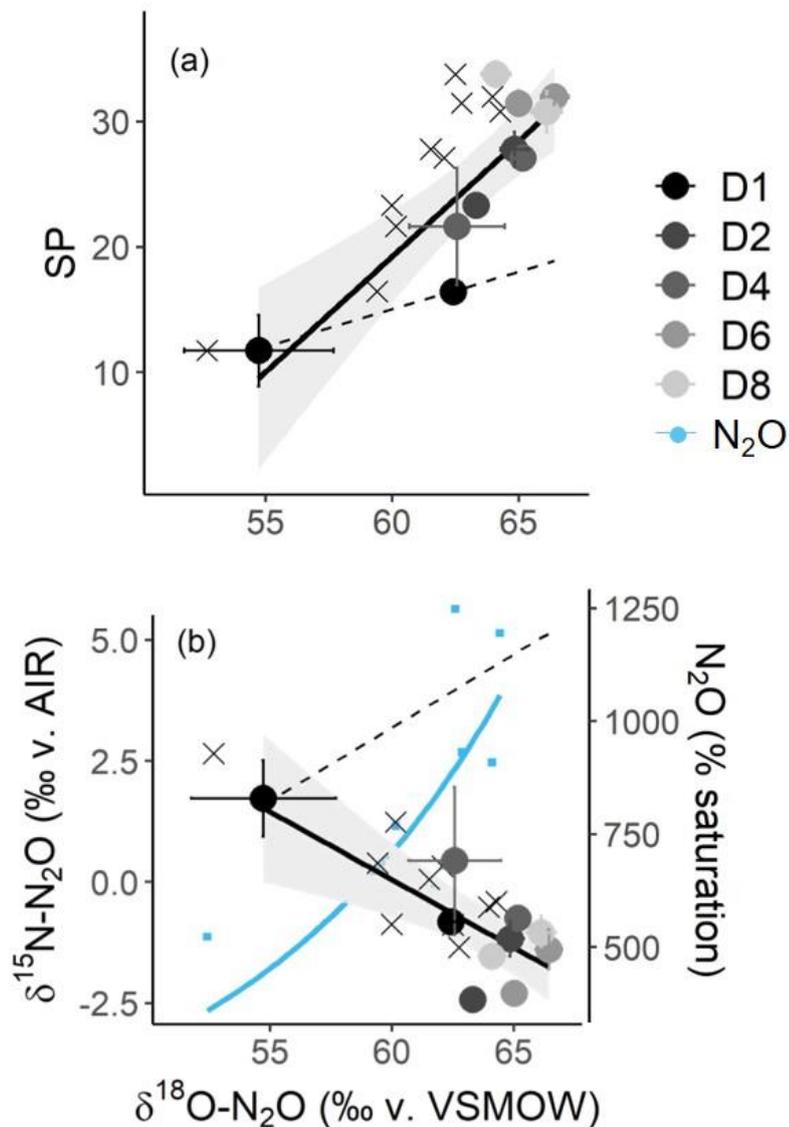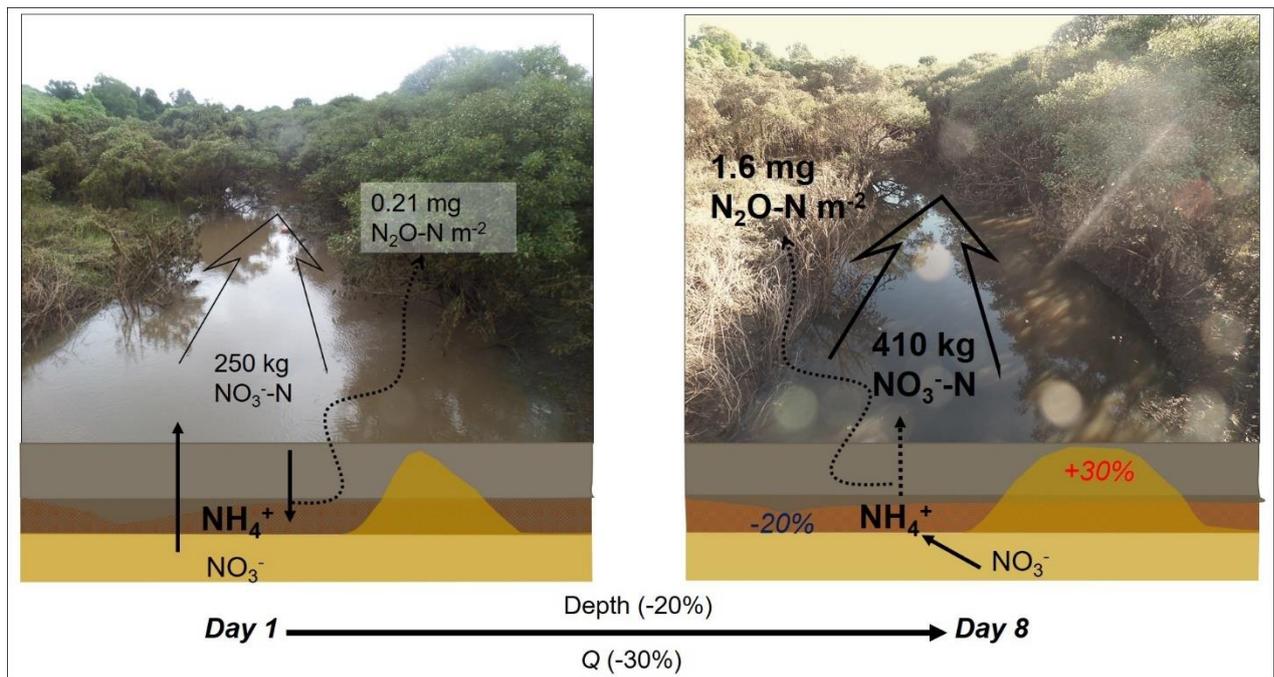
732

733

734

735

736

737

Figure 6

739

Fig. 6 The isotopic composition of surface water N_2O, measured over eight days as stream
flow declined (D1 → D8). Each $\delta^{15}N$-N_2O, $\delta^{18}O$-N_2O and ^{15}N site preference (SP) value
represent the mean ± SD of samples collected at nine locations across the width and length of
a stream reach; measurements were carried out twice during each 24-hr period. The $\delta^{18}O$-
N_2O values are corrected for mixing with atmospheric N_2O (Eq. 1); crosses represent
uncorrected values. Solid lines represent the best-fit of the linear regression between $\delta^{18}O$-
N_2O and SP (a; y = -56 + 1.3x, $p<0.001$, $r^2 = 0.61$) and $\delta^{15}N$-N_2O and $\delta^{18}O$-N_2O (b; y = 16 –
0.26x, $p<0.001$, $r^2 = 0.45$), with grey shading over the 95% CI. Dashed lines indicate the SP
v $\delta^{18}O$-N_2O (a) and $\delta^{15}N$-N_2O v $\delta^{18}O$-N_2O (b) relationships produced during N_2O reduction
to N_2 (Lewicka-Szczebak et al., 2017; Ostrom et al., 2007). The mean surface water N_2O
saturation for the three hours around each sampling point is shown (blue points and line).

751

752

Figure 7

Depth (-20%)
Day 1 ⟶ **Day 8**
Q (-30%)

Fig. 7 Over eight days the surface water depth and discharge (*Q*) decreased, causing surface waters to become more groundwater (yellow) dominated as it returned toward baseflow, and less surface water (brown) reached the hyporheic sediment zone (orange). The combination of decreased exchange and increased residence time enhanced biological oxidation of the large sediment NH_4^+ pool, increasing water-air N_2O emissions and downstream NO_3^- discharge. Photos are from two days prior to D1 (left) and on D6 (right), credit: N.S. Wells.

References

Alexander, R.B., Bohlke, J.K., Boyer, E.W., David, M.B., Harvey, J.W., Mulholland, P.J., Seitzinger, S.P., Tobias, C.R., Tonitto, C. and Wollheim, W.M. (2009) Dynamic modeling of nitrogen losses in river networks unravels the coupled effects of hydrological and biogeochemical processes. *Biogeochem.* **93**, 91-116.

Appling, A.P., Hall Jr., R.O., Yackulic, C.B. and Arroita, M. (2018) Overcoming equifinality: Leveraging long time series for stream metabolism estimation. *J. Geophys. Res- Biogeosci.* **123**, 624-645.

Appling, A.P. and Heffernan, J.B. (2014) Nutrient limitation and physiology mediate the fine-scale (de)coupling of biogeochemical cycles. *Am. Nat.* **184**, 384-406.

Atkins, M.L., Santos, I.R., Ruiz-Halpern, S. and Maher, D.T. (2013) Carbon dioxide dynamics driven by groundwater discharge in a coastal floodplain creek. *J. Hydrol.* **493**, 30-42.

Azizian, M., Boano, F., Cook, P.L.M., Detwiler, R.L., Rippy, M.A. and Grant, S.B. (2017) Ambient groundwater flow diminishes nitrate processing in the hyporheic zone of streams. *Water Resour. Res.* **53**, 3941-3967.

Barnes, R.T., Sawyer, A.H., Tight, D.M., Wallace, C.D. and Hastings, M.G. (2019) Hydrogeologic controls of surface water-groundwater nitrogen dynamics within a tidal freshwater zone. *J. Geophys. Res- Biogeosci.* **124**.

Bates, D., Mächler, M., Bolker, B. and Walker, S. (2015) Fitting linear mixed-effects models using lme4. *Journal of Statistical Software* **67**, 48.

Baulch, H.M., Dillon, P.J., Maranger, R., Venkiteswaran, J.J., Wilson, H.F. and Schiff, S.L. (2012) Night and day: short-term variation in nitrogen chemistry and nitrous oxide emissions from streams. *Freshwater Biol.* **57**, 509-525.

Beaulieu, J.J., Tank, J.L., Hamilton, S.K., Wollheim, W.M., Hall, R.O., Mulholland, P.J., Peterson, B.J., Ashkenas, L.R., Cooper, L.W., Dahm, C.N., Dodds, W.K., Grimm, N.B., Johnson, S.L., McDowell, W.H., Poole, G.C., Valett, H.M., Arango, C.P., Bernot, M.J., Burgin, A.J., Crenshaw, C.L., Helton, A.M., Johnson, L.T., O'Brien, J.M., Potter, J.D., Sheibley, R.W., Sobota, D.J. and Thomas, S.M. (2011) Nitrous oxide emission from denitrification in stream and river networks. *P. Natl. Acad. Sci. USA* **108**, 214-219.

Bernhardt, E.S., Heffernan, J.B., Grimm, N.B., Stanley, E.H., Harvey, J.W., Arroita, M., Appling, A.P., Cohen, M.J., McDowell, W.H., Hall, R.O., Read, J.S., Roberts, B.J., Stets, E.G. and Yackulic, C.B. (2018) The metabolic regimes of flowing waters. *Limnol. Oceanograph.* **63**, S99-S118.

Bianchin, M.S., Smith, L. and Beckie, R.D. (2011) Defining the hyporheic zone in a large tidally influenced river. *J. Hydrol.* **406**, 16-29.

Bormans, M., Ford, P.W., Fabbro, L. and Hancock, G. (2004) Onset and persistence of cyanobacterial blooms in a large impounded tropical river, Australia. *Marine and Freshwater Research* **55**, 1-15.

Boshers, D.S., Granger, J., Tobias, C.R., Böhlke, J.K. and Smith, R.L. (2019) Constraining the oxygen isotopic composition of nitrate produced by nitrification. *Environ. Sci. Technol.* **53**, 1206-1216.

Boyer, E.W., Howarth, R.W., Galloway, J.N., Dentener, F.J., Green, P.A. and Vörösmarty, C.J. (2006) Riverine nitrogen export from the continents to the coasts. *Global Biogeochem. Cy.* **20**, n/a-n/a.

Briggs, M.A., Day-Lewis, F.D., Zarnetske, J.P. and Harvey, J.W. (2015) A physical explanation for the development of redox microzones in hyporheic flow. *Geophysical Research Letters* **42**, 4402-4410.

Briggs, M.A., Lautz, L.K. and Hare, D.K. (2014) Residence time control on hot moments of net nitrate production and uptake in the hyporheic zone. *Hydrol. Process.* **28**, 3741-3751.

Brodie, R., Sundaram, B., Tottenham, R., Hostetler, S. and Ransley, T. (2007) An overview of tools for assessing groundwater-surface water connectivity Bureau of Rural Sciences. Bureau of Rural Sciences, Canberra

Brodie, R.S., Green, R. and Graham, M. (2003) Mapping groundwater-dependent ecosystems: a case study in the fractured basalt aquifers of the Alstonville Plateau, New South Wales, Australia.

Buchwald, C., Santoro, A.E., McIlvin, M.R. and Casciotti, K.L. (2012) Oxygen isotopic composition of nitrate and nitrite produced by nitrifying cocultures and natural marine assemblages. *Limnol. Oceanograph.* **57**, 1361-1375.

Burnett, W.C., Peterson, R.N., Santos, I.R. and Hicks, R.W. (2010) Use of automated radon measurements for rapid assessment of groundwater flow into Florida streams. *J. Hydrol.* **380**, 298-304.

Call, M., Maher, D.T., Santos, I.R., Ruiz-Halpern, S., Mangion, P., Sanders, C.J., Erler, D.V., Oakes, J.M., Rosentreter, J., Murray, R. and Eyre, B.D. (2015) Spatial and temporal variability of carbon dioxide and methane fluxes over semi-diurnal and spring-neap-spring timescales in a mangrove creek. *Geochim Cosmochim Ac* **150**, 211-225.

Casciotti, K.L., Sigman, D.M. and Ward, B.B. (2003) Linking diversity and stable isotope fractionation in ammonia-oxidizing bacteria. *Geomicrobiol. J.* **20**, 335-353.

Chamberlin, C.A., Bernhardt, E.S., Rosi, E.J. and Heffernan, J.B. (2019) Stoichiometry and daily rhythms: experimental evidence shows nutrient limitation decouples N uptake from photosynthesis. *Ecology* **100**, e02822.

Chen, X.L., Tague, C.L., Melack, J.M. and Keller, A.A. (2020) Sensitivity of nitrate concentration-discharge patterns to soil nitrate distribution and drainage properties in the vertical dimension. *Hydrol. Process.*, 17.

Christensen, P.B., Nielsen, L.P., Sorensen, J. and Revsbech, N.P. (1990) Denitrification in nitrate-rich streams - Diurnal and seasonal - variation related to benthic oxygen-metabolism. *Limnol. Oceanograph.* **35**, 640-651.

Clough, T.J., Buckthought, L.E., Kelliher, F.M. and Sherlock, R.R. (2007) Diurnal fluctuations of dissolved nitrous oxide (N_2O) concentrations and estimates of N_2O emissions from a spring-fed river: implications for IPCC methodology. *Global Change Biol.* **13**, 1016-1027.

Cohen, M.J., Heffernan, J.B., Albertin, A. and Martin, J.B. (2012) Inference of riverine nitrogen processing from longitudinal and diel variation in dual nitrate isotopes. *J. Geophys. Res.-Biogeosci.* **117**, 17.

Comer-Warner, S., Knapp, J.L.A., Blaen, P., Klaar, M., Shelley, F., Zarnetske, J., Lee-Cullin, J., Folegot, S., Kurz, M., Lewandowski, J., Harvey, J., Ward, A., Mendoza-Lera, C., Ullah, S., Datry, T., Kettridge, N., Gooddy, D., Drummond, J., Martí, E., Milner, A., Hannah, D. and Krause, S. (2020a) The method controls the story - Sampling method impacts on the detection of pore-water nitrogen concentrations in streambeds. *Sci. Total Environ.* **709**, 136075.

Comer-Warner, S.A., Gooddy, D.C., Ullah, S., Glover, L., Kettridge, N., Wexler, S.K., Kaiser, J. and Krause, S. (2020b) Seasonal variability of sediment controls of nitrogen cycling in an agricultural stream. *Biogeochem.* **148**, 31-48.

Comer-Warner, S.A., Krause, S., Gooddy, D.C., Bennett, S.A., Wexler, S.K. and Kaiser, J. (2017) Opening opportunities for high-resolution isotope analysis - Quantification of delta N-15(NO3) and delta O-18(NO3) in diffusive equilibrium in thin-film passive samplers. *Anal. Chem.* **89**, 4139-4146.

Covino, T.P., Bernhardt, E.S. and Heffernan, J.B. (2018) Measuring and interpreting relationships between nutrient supply, demand, and limitation. *Freshwater Sci.* **37**, 448-455.

Denk, T.R.A., Mohn, J., Decock, C., Lewicka-Szczebak, D., Harris, E., Butterbach-Bahl, K., Kiese, R. and Wolf, B. (2017) The nitrogen cycle: A review of isotope effects and isotope modeling approaches. *Soil Biol. Biochem.* **105**, 121-137.

Dudley-Southern, M. and Binley, A. (2015) Temporal responses of groundwater-surface water exchange to successive storm events. *Water Resour. Res.* **51**, 1112-1126.

Erler, D.V., Duncan, T.M., Murray, R., Maher, D.T., Santos, I.R., Gatland, J.R., Mangion, P. and Eyre, B.D. (2015) Applying cavity ring-down spectroscopy for the measurement of dissolved nitrous oxide concentrations and bulk nitrogen isotopic composition in aquatic systems: Correcting for interferences and field application. *Limnology & Oceanography: Methods* **13**, 391-401.

Eyre, B.D. and Ferguson, A.J.P. (2009) Denitrification efficiency for defining critical loads of carbon in shallow coastal ecosystems. *Hydrobiologia* **629**, 137-146.

876   Eyre, B.D. and Pont, D. (2003) Intra- and inter-annual variability in the different forms of diffuse
877   nitrogen and phosphorus delivered to seven sub-tropical east Australian estuaries. *Estuarine,*
878   *Coastal and Shelf Science* **57**, 137-148.
879   Fang, Y., Koba, K., Makabe, A., Zhu, F., Fan, S., Liu, X. and Yoh, M. (2012) Low $\delta^{18}O$ values of
880   nitrate produced from nitrification in temperate forest soils. *Environ. Sci. Technol.* **46**, 8723-
881   8730.
882   Fork, M.L. and Heffernan, J.B. (2014) Direct and indirect effects of dissolved organic matter source
883   and concentration on denitrification in northern Florida rivers. *Ecosystems* **17**, 14-28.
884   Fowler, D., Coyle, M., Skiba, U., Sutton, M.A., Cape, J.N., Reis, S., Sheppard, L.J., Jenkins, A.,
885   Grizzetti, B., Galloway, J.N., Vitousek, P., Leach, A., Bouwman, A.F., Butterbach-Bahl, K.,
886   Dentener, F., Stevenson, D., Amann, M. and Voss, M. (2013) The global nitrogen cycle in the
887   twenty-first century. *Philosophical Transactions of the Royal Society B: Biological Sciences*
888   **368**, 20130164.
889   Frame, C.H. and Casciotti, K.L. (2010) Biogeochemical controls and isotopic signatures of nitrous
890   oxide production by a marine ammonia-oxidizing bacterium. *Biogeosci.* **7**, 2695-2709.
891   Galloway, J.N., Townsend, A.R., Erisman, J.W., Bekunda, M., Cai, Z., Freney, J.R., Martinelli, L.A.,
892   Seitzinger, S.P. and Sutton, M.A. (2008) Transformation of the nitrogen cycle: Recent trends,
893   questions, and potential solutions. *Science* **320**, 889-892.
894   Gatland, J.R., Santos, I.R., Maher, D.T., Duncan, T.M. and Erler, D.V. (2014) Carbon dioxide and
895   methane emissions from an artificially drained coastal wetland during a flood: Implications
896   for wetland global warming potential. *J. Geophys. Res.-Biogeosci.* **119**, 1698-1716.
897   Gomez-Velez, J.D., Harvey, J., Cardenas, M.B. and Kiel, B. (2015) Denitrification in the Mississippi
898   River network controlled by flow through river bedforms. *Nat. Geosci.* **8**, 941-U975.
899   Granger, J. and Wankel, S.D. (2016) Isotopic overprinting of nitrification on denitrification as a
900   ubiquitous and unifying feature of environmental nitrogen cycling. *Proc Natl Acad Sci U S A*
901   **113**, E6391-E6400.
902   Gupta, G. and Karuppiah, M. (1996) Toxicity study of a Chesapeake Bay tributary - Wicomico River.
903   *Chemosphere* **32**, 1193-1215.
904   Hall, R.O. and Tank, J.L. (2003) Ecosystem metabolism controls nitrogen uptake in streams in Grand
905   Teton National Park, Wyoming. *Limnol. Oceanograph.* **48**, 1120-1128.
906   Hall, R.O. and Ulseth, A.J. (2019) Gas exchange in streams and rivers. *WIREs Water* **0**, e1391.
907   Hampton, T.B., Zarnetske, J.P., Briggs, M.A., Dehkordy, F.M., Singha, K., Day-Lewis, F.D., Harvey,
908   J.W., Chowdhury, S.R. and Lane, J.W. (2020) Experimental shifts of hydrologic residence
909   time in a sandy urban stream sediment-water interface alter nitrate removal and nitrous oxide
910   fluxes. *Biogeochem.* **149**, 195–219.
911   Harrison, J. and Matson, P. (2003) Patterns and controls of nitrous oxide emissions from waters
912   draining a subtropical agricultural valley. *Global Biogeochem. Cy.* **17**, 13.
913   Harrison, J.A., Matson, P.A. and Fendorf, S.E. (2005) Effects of a diel oxygen cycle on nitrogen
914   transformations and greenhouse gas emissions in a eutrophied subtropical stream. *Aquat. Sci.*
915   **67**, 308-315.
916   Harvey, J.W., Bohlke, J.K., Voytek, M.A., Scott, D. and Tobias, C.R. (2013) Hyporheic zone
917   denitrification: Controls on effective reaction depth and contribution to whole-stream mass
918   balance. *Water Resour. Res.* **49**, 6298-6316.
919   Haslun, J.A., Ostrom, N.E., Hegg, E.L. and Ostrom, P.H. (2018) Estimation of isotope variation of
920   N_2O during denitrification by Pseudomonas aureofaciens and Pseudomonas chlororaphis:
921   implications for N_2O source apportionment. *Biogeosci.* **15**, 3873-3882.
922   Hester, E.T., Eastes, L.A. and Widdowson, M.A. (2019) Effect of surface water stage fluctuation on
923   mixing-dependent hyporheic denitrification in riverbed dunes. *Water Resour. Res.* **55**, 4668-
924   4687.
925   Hu, M.P., Chen, D.J. and Dahlgren, R.A. (2016) Modeling nitrous oxide emission from rivers: A
926   global assessment. *Global Change Biol.* **22**, 3566-3582.
927   Huang, J., Bennett, W.W., Welsh, D.T., Li, T. and Teasdale, P.R. (2016) "Diffusive Gradients in Thin
928   Films" techniques provide representative time-weighted average measurements of inorganic
929   nutrients in dynamic freshwater systems. *Environ. Sci. Technol.* **50**, 13446-13454.

930 Huang, J.Y., Franklin, H., Teasdale, P.R., Burford, M.A., Kankanamge, N.R., Bennett, W.W. and
931   Welsh, D.T. (2019) Comparison of DET, DGT and conventional porewater extractions for
932   determining nutrient profiles and cycling in stream sediments. *Environ. Sci.-Process Impacts*
933   **21**, 2128-2140.
934 Ji, Q.X., Frey, C., Sun, X., Jackson, M., Lee, Y.S., Jayakumar, A., Cornwell, J.C. and Ward, B.B.
935   (2018) Nitrogen and oxygen availabilities control water column nitrous oxide production
936   during seasonal anoxia in the Chesapeake Bay. *Biogeosci.* **15**, 6127-6138.
937 Julian, J.P., Davies-Colley, R.J., Gallegos, C.L. and Tran, T.V. (2013) Optical water quality of inland
938   waters: a landscape perspective. *Ann. Assoc. Am. Geogr.* **103**, 309-318.
939 Kassambara, A. (2020) ggpubr: 'ggplot2' Based Publication Ready Plots, R package version 0.3.0 ed,
940   https://CRAN.R-project.org/package=ggpubr.
941 Kendall, C. (1998) Tracing nitrogen sources and cycling in catchments, in: Kendall, C., Mcdonell, J.J.
942   (Eds.), Isotope Tracers in Catchment Hydrology. Elsevier Science B.V., Amsterdam, pp. 519-
943   576.
944 Kessler, A.J., Glud, R.N., Cardenas, M.B. and Cook, P.L.M. (2013) Transport zonation limits coupled
945   nitrification-denitrification in permeable sediments. *Environ. Sci. Technol.* **47**, 13404-13411.
946 Khadka, M.B., Martin, J.B. and Kurz, M.J. (2017) Synoptic estimates of diffuse groundwater seepage
947   to a spring-fed karst river at high spatial resolution using an automated radon measurement
948   technique. *J. Hydrol.* **544**, 86-96.
949 Knights, D., Sawyer, A.H., Barnes, R.T., Musial, C.T. and Bray, S. (2017) Tidal controls on riverbed
950   denitrification along a tidal freshwater zone. *Water Resour. Res.* **53**, 799-816.
951 Knowles, J.E. and Frederick, C. (2019) merTools: Tools for Analyzing Mixed Effect Regression
952   Models, R package version 0.5.0 ed, https://CRAN.R-project.org/package=merTools.
953 Krause, S., Lewandowski, J., Grimm, N.B., Hannah, D.M., Pinay, G., McDonald, K., Martí, E.,
954   Argerich, A., Pfister, L., Klaus, J., Battin, T., Larned, S.T., Schelker, J., Fleckenstein, J.,
955   Schmidt, C., Rivett, M.O., Watts, G., Sabater, F., Sorolla, A. and Turk, V. (2017)
956   Ecohydrological interfaces as hotspots of ecosystem processes. *Water Resour. Res.*, n/a-n/a.
957 Kroeze, C., Dumont, E. and Seitzinger, S.P. (2005) New estimates of global emissions of N_2O from
958   rivers and estuaries. *Environmental Sciences* **2**, 159-165.
959 Kroopnick, P. and Craig, H. (1972) Atmospheric oxygen: isotopic composition and solubility
960   fractionation. *Science* **175**, 54-55.
961 Laursen, A.E. and Seitzinger, S.P. (2004) Diurnal patterns of denitrification, oxygen consumption and
962   nitrous oxide production in rivers measured at the whole-reach scale. *Freshwater Biol.* **49**,
963   1448-1458.
964 Lewandowski, J., Arnon, S., Banks, E., Batelaan, O., Betterle, A., Broecker, T., Coll, C., Drummond,
965   J.D., Garcia, J.G., Galloway, J., Gomez-Velez, J., Grabowski, R.C., Herzog, S.P.,
966   Hinkelmann, R., Hohne, A., Hollender, J., Horn, M.A., Jaeger, A., Krause, S., Prats, A.L.,
967   Magliozzi, C., Meinikmann, K., Mojarrad, B.B., Mueller, B.M., Peralta-Maraver, I., Popp,
968   A.L., Posselt, M., Putschew, A., Radke, M., Raza, M., Riml, J., Robertson, A., Rutere, C.,
969   Schaper, J.L., Schirmer, M., Schulz, H., Shanafield, M., Singh, T., Ward, A.S., Wolke, P.,
970   Worman, A. and Wu, L.W. (2019) Is the hyporheic zone relevant beyond the scientific
971   community? *Water* **11**, 32.
972 Lewicka-Szczebak, D., Augustin, J., Giesemann, A. and Well, R. (2017) Quantifying N_2O reduction
973   to N_2 based on N_2O isotopocules - validation with independent methods (helium incubation
974   and ^{15}N gas flux method). *Biogeosci.* **14**, 22.
975 Looman, A., Santos, I.R., Tait, D.R., Webb, J.R., Sullivan, C.A. and Maher, D.T. (2016) Carbon
976   cycling and exports over diel and flood-recovery timescales in a subtropical rainforest
977   headwater stream. *Sci. Total Environ.* **550**, 645-657.
978 Maher, D.T., Santos, I.R., Leuven, J.R.F.W., Oakes, J.M., Erler, D.V., Carvalho de Carvalho, M. and
979   Eyre, B.D. (2013) Novel use of cavity ring-down spectroscopy to investigate aquatic carbon
980   cycling from microbial to ecosystem scales. *Environ. Sci. Technol.* **47**, 12938-12945.
981 Marcé, R., von Schiller, D., Aguilera, R., Martí, E. and Bernal, S. (2018) Contribution of hydrologic
982   opportunity and biogeochemical reactivity to the variability of nutrient retention in river
983   networks. *Global Biogeochem. Cy.* **32**, 376-388.

984　Martí, E., Feijoó, C., Vilches, C., Ferreiro, N., Gantes, P., Ranieri, C., Torremorell, A., Castro,
985　　　　M.C.R., Gultemiriam, M.L., Giorgi, A. and Sabater, F. (2020) Diel variation of nutrient
986　　　　retention is associated with metabolism for ammonium but not phosphorus in a lowland
987　　　　stream. *Freshwater Sci.* **0**, 000-000.
988　Marzadri, A., Dee, M.M., Tonina, D., Bellin, A. and Tank, J.L. (2017) Role of surface and subsurface
989　　　　processes in scaling N_2O emissions along riverine networks. *Proc Natl Acad Sci U S A* **114**,
990　　　　4330-4335.
991　McCrackin, M.L., Harrison, J.A. and Compton, J.E. (2014) Factors influencing export of dissolved
992　　　　inorganic nitrogen by major rivers: A new, seasonal, spatially explicit, global model. *Global*
993　　　　*Biogeochem. Cy.* **28**, 269-285.
994　McIlvin, M.R. and Casciotti, K.L. (2011) Technical updates to the bacterial method for nitrate
995　　　　isotopic analyses. *Anal. Chem.* **83**, 1850-1856.
996　McKee, L., Eyre, B. and Hossain, S. (2000) Intra- and interannual export of nitrogen and phosphorus
997　　　　in the subtropical Richmond River catchment, Australia. *Hydrol. Process.* **14**, 1787-1809.
998　McMahon, P.B. and Dennehy, K.F. (1999) N_2O emissions from a nitrogen-enriched river. *Environ.*
999　　　　*Sci. Technol.* **33**, 21-25.
1000　Mohn, J., Wolf, B., Toyoda, S., Lin, C.-T., Liang, M.-C., Brüggemann, N., Wissel, H., Steiker, A.E.,
1001　　　　Dyckmans, J., Szwec, L., Ostrom, N.E., Casciotti, K.L., Forbes, M., Giesemann, A., Well, R.,
1002　　　　Doucett, R.R., Yarnes, C.T., Ridley, A.R., Kaiser, J. and Yoshida, N. (2014) Interlaboratory
1003　　　　assessment of nitrous oxide isotopomer analysis by isotope ratio mass spectrometry and laser
1004　　　　spectroscopy: current status and perspectives. *Rapid Communications in Mass Spectrometry*
1005　　　　**28**, 1995-2007.
1006　Morgan, B., Rate, A.W. and Burton, E.D. (2012) Water chemistry and nutrient release during the
1007　　　　resuspension of FeS-rich sediments in a eutrophic estuarine system. *Sci. Total Environ.* **432**,
1008　　　　47-56.
1009　Murray, R., Erler, D., Rosentreter, J., Maher, D. and Eyre, B. (2018) A seasonal source and sink of
1010　　　　nitrous oxide in mangroves: Insights from concentration, isotope, and isotopomer
1011　　　　measurements. *Geochim Cosmochim Ac* **238**, 169-192.
1012　Murray, R.H., Erler, D.V. and Eyre, B.D. (2015) Nitrous oxide fluxes in estuarine environments:
1013　　　　Response to global change. *Global Change Biol.* **21**, 3219-3245.
1014　Naranjo, R.C., Niswonger, R.G. and Davis, C.J. (2015) Mixing effects on nitrogen and oxygen
1015　　　　concentrations and the relationship to mean residence time in a hyporheic zone of a riffle-pool
1016　　　　sequence. *Water Resour. Res.* **51**, 7202-7217.
1017　O'Donnell, B. and Hotchkiss, E.R. (2019) Coupling concentration- and process-discharge
1018　　　　relationships integrates water chemistry and metabolism in streams. *Water Resour. Res.* **55**,
1019　　　　12.
1020　Ocampo, C.J., Oldham, C.E., Sivapalan, M. and Turner, J.V. (2006) Hydrological versus
1021　　　　biogeochemical controls on catchment nitrate export: a test of the flushing mechanism.
1022　　　　*Hydrol. Process.* **20**, 4269-4286.
1023　Oliver, R.L., Mitrovic, S.M. and Rees, C. (2010) Influence of salinity on light conditions and
1024　　　　phytoplankton growth in a turbid river. *River Research and Applications* **26**, 894-903.
1025　Ostrom, N.E. and Ostrom, P.H. (2017) Mining the isotopic complexity of nitrous oxide: a review of
1026　　　　challenges and opportunities. *Biogeochem.* **132**, 359-372.
1027　Ostrom, N.E., Pitt, A., Sutka, R., Ostrom, P.H., Grandy, A.S., Huizinga, K.M. and Robertson, G.P.
1028　　　　(2007) Isotopologue effects during N_2O reduction in soils and in pure cultures of denitrifiers.
1029　　　　*J. Geophys. Res.-Biogeosci.* **112**, 12.
1030　Palmer-Felgate, E.J., Mortimer, R.J.G., Krom, M.D. and Jarvie, H.P. (2010) Impact of point-source
1031　　　　pollution on phosphorus and nitrogen cycling in stream-bed sediments. *Environ. Sci. Technol.*
1032　　　　**44**, 908-914.
1033　Parker, S.R., Poulson, S.R., Gammons, C.H. and DeGrandpre, M.D. (2005) Biogeochemical controls
1034　　　　on diel cycling of stable isotopes of dissolved O_2 and dissolved inorganic carbon in the Big
1035　　　　Hole River, Montana. *Environ. Sci. Technol.* **39**, 7134-7140.
1036　Pedersen, T.L. (2019) patchwork: The Composer of Plots, R package version 1.0.0 ed,
1037　　　　https://CRAN.R-project.org/package=patchwork.

Quick, A.M., Reeder, W.J., Farrell, T.B., Tonina, D., Feris, K.P. and Benner, S.G. (2016) Controls on nitrous oxide emissions from the hyporheic zones of streams. *Environ. Sci. Technol.* **50**, 11491-11500.

Quick, A.M., Reeder, W.J., Farrell, T.B., Tonina, D., Feris, K.P. and Benner, S.G. (2019) Nitrous oxide from streams and rivers: A review of primary biogeochemical pathways and environmental variables. *Earth-Sci. Rev.* **191**, 224-262.

Rahimi, M., Essaid, H.I. and Wilson, J.T. (2015) The role of dynamic surface water-groundwater exchange on streambed denitrification in a first-order, low-relief agricultural watershed. *Water Resour. Res.* **51**, 9514-9538.

Raymond, P.A., Saiers, J.E. and Sobczak, W.V. (2016) Hydrological and biogeochemical controls on watershed dissolved organic matter transport: pulse-shunt concept. *Ecology* **97**, 5-16.

Raymond, P.A., Zappa, C.J., Butman, D., Bott, T.L., Potter, J., Mulholland, P., Laursen, A.E., McDowell, W.H. and Newbold, D. (2012) Scaling the gas transfer velocity and hydraulic geometry in streams and small rivers. *Limnology & Oceanography: Fluids and Environments* **2**, 41-53.

Reading, M.J., Santos, I.R., Maher, D.T., Jeffrey, L. and Tait, D.R. (2017) Shifting nitrous oxide source/sink behaviour in a subtropical estuary revealed by automated time series observations. *Estuarine, Coastal and Shelf Science* **194**, 66-76.

Reisinger, A.J., Doody, T.R., Groffman, P.M., Kaushal, S.S. and Rosi, E.J. (2019) Seeing the light: urban stream restoration affects stream metabolism and nitrate uptake via changes in canopy cover. *Ecol. Appl.* **29**, 15.

Reisinger, A.J., Tank, J.L., Hoellein, T.J. and Hall, R.O. (2016) Sediment, water column, and open-channel denitrification in rivers measured using membrane-inlet mass spectrometry. *J. Geophys. Res.-Biogeosci.* **121**, 1258-1274.

Rosamond, M.S., Thuss, S.J. and Schiff, S.L. (2012) Dependence of riverine nitrous oxide emissions on dissolved oxygen levels. *Nat. Geosci.* **5**, 715.

Rosamond, M.S., Thuss, S.J., Schiff, S.L. and Elgood, R.J. (2011) Coupled cycles of dissolved oxygen and nitrous oxide in rivers along a trophic gradient in southern Ontario, Canada. *J. Environ. Qual.* **40**, 256-270.

Salk, K.R., Ostrom, P.H., Biddanda, B.A., Weinke, A.D., Kendall, S.T. and Ostrom, N.E. (2016) Ecosystem metabolism and greenhouse gas production in a mesotrophic northern temperate lake experiencing seasonal hypoxia. *Biogeochem.* **131**, 303-319.

Santos, I.R., Maher, D.T. and Eyre, B.D. (2012) Coupling automated radon and carbon dioxide measurements in coastal waters. *Environ. Sci. Technol.* **46**, 7685-7691.

Schubert, M. and Paschke, A. (2015) Radon, CO_2 and CH_4 as environmental tracers in groundwater/surface water interaction studies - comparative theoretical evaluation of the gas specific water/air phase transfer kinetics. *Eur. Phys. J.-Spec. Top.* **224**, 709-715.

Schutte, C.A., Joye, S.B., Wilson, A.M., Evans, T., Moore, W.S. and Casciotti, K. (2015) Intense nitrogen cycling in permeable intertidal sediment revealed by a nitrous oxide hot spot. *Global Biogeochem. Cy.* **29**, 1584-1598.

Seitzinger, S., Harrison, J.A., Bohlke, J.K., Bouwman, A.F., Lowrance, R., Peterson, B., Tobias, C. and Van Drecht, G. (2006) Denitrification across landscapes and waterscapes: A synthesis. *Ecol. Appl.* **16**, 2064-2090.

Singh, T., Wu, L.W., Gomez-Velez, J.D., Lewandowski, J., Hannah, D.M. and Krause, S. (2019) Dynamic hyporheic zones: exploring the role of peak flow events on bedform-induced hyporheic exchange. *Water Resour. Res.* **55**, 218-235.

Smith, J.M., Chavez, F.P. and Francis, C.A. (2014) Ammonium uptake by phytoplankton regulates nitrification in the sunlit ocean. *PloS one* **9**, 9.

Snider, D.M., Schiff, S.L. and Spoelstra, J. (2009) N-15/N-14 and O-18/O-16 stable isotope ratios of nitrous oxide produced during denitrification in temperate forest soils. *Geochim Cosmochim Ac* **73**, 877-888.

Snider, D.M., Venkiteswaran, J.J., Schiff, S.L. and Spoelstra, J. (2013) A new mechanistic model of δ^{18}O-N$_2$O formation by denitrification. *Geochim Cosmochim Ac* **112**, 102-115.

1091 Stanley, E.H., Casson, N.J., Christel, S.T., Crawford, J.T., Loken, L.C. and Oliver, S.K. (2016) The
1092   ecology of methane in streams and rivers: patterns, controls, and global significance. *Ecol.*
1093   *Monogr.* **86**, 146-171.
1094 Stephens, B.M., Wankel, S.D., Beman, J.M., Rabines, A.J., Allen, A.E. and Aluwihare, L.I. (2019)
1095   Euphotic zone nitrification in the California Current Ecosystem. *Limnol. Oceanograph.* **9999**,
1096   1-17.
1097 Tank, J.L., Rosi-Marshall, E.J., Griffiths, N.A., Entrekin, S.A. and Stephen, M.L. (2010) A review of
1098   allochthonous organic matter dynamics and metabolism in streams. *J. N. Am. Benthol. Soc.*
1099   **29**, 118-146.
1100 Thuss, S.J., Venkiteswaran, J.J. and Schiff, S.L. (2014) Proper interpretation of dissolved nitrous
1101   oxide isotopes, production pathways, and emissions requires a modelling approach. *PloS one*
1102   **9**, 15.
1103 Toyoda, S. and Yoshida, N. (1999) Determination of nitrogen isotopomers of nitrous oxide on a
1104   modified isotope ratio mass spectrometer. *Anal. Chem.* **71**, 4711-4718.
1105 Trauth, N. and Fleckenstein, J.H. (2017) Single discharge events increase reactive efficiency of the
1106   hyporheic zone. *Water Resour. Res.* **53**, 779-798.
1107 Trauth, N., Schmidt, C., Vieweg, M., Maier, U. and Fleckenstein, J.H. (2014) Hyporheic transport and
1108   biogeochemical reactions in pool-riffle systems under varying ambient groundwater flow
1109   conditions. *J. Geophys. Res.-Biogeosci.* **119**, 910-928.
1110 Trimmer, M., Grey, J., Heppell, C.M., Hildrew, A.G., Lansdown, K., Stahl, H. and Yvon-Durocher,
1111   G. (2012) River bed carbon and nitrogen cycling: State of play and some new directions. *Sci.*
1112   *Total Environ.* **434**, 143-158.
1113 Turner, P.A., Griffis, T.J., Lee, X.H., Baker, J.M., Venterea, R.T. and Wood, J.D. (2015) Indirect
1114   nitrous oxide emissions from streams within the US Corn Belt scale with stream order. *Proc*
1115   *Natl Acad Sci U S A* **112**, 9839-9843.
1116 Tysmans, D.J.J., Lohr, A.J., Kroeze, C., Ivens, W. and van Wijnen, J. (2013) Spatial and temporal
1117   variability of nutrient retention in river basins: A global inventory. *Ecol. Indic.* **34**, 607-615.
1118 Venkiteswaran, J.J., Rosamond, M.S. and Schiff, S.L. (2014) Nonlinear response of riverine N_2O
1119   fluxes to oxygen and temperature. *Environ. Sci. Technol.* **48**, 1566-1573.
1120 Wanninkhof, R. (2014) Relationship between wind speed and gas exchange over the ocean revisited.
1121   *Limnology & Oceanography: Methods* **12**, 351-362.
1122 Webb, J.R., Santos, I.R., Robson, B., Macdonald, B., Jeffrey, L. and Maher, D.T. (2017) Constraining
1123   the annual groundwater contribution to the water balance of an agricultural floodplain using
1124   radon: The importance of floods. *Water Resour. Res.* **53**, 544-562.
1125 Weiss, R.F. and Price, B.A. (1980) Nitrous-oxide solubility in water and seawater. *Mar. Chem.* **8**,
1126   347-359.
1127 Well, R., Eschenbach, W., Flessa, H., von der Heide, C. and Weymann, D. (2012) Are dual isotope
1128   and isotopomer ratios of N_2O useful indicators for N_2O turnover during denitrification in
1129   nitrate-contaminated aquifers? *Geochim Cosmochim Ac* **90**, 265-282.
1130 Wells, N.S., Baisden, W.T., Clough, T.J., Johnson-Beebout, S.E. and Elberling, B. (2019) Effects of
1131   denitrification and transport on the isotopic composition of nitrate ($\delta^{18}O$, $\delta^{15}N$) in freshwater
1132   systems. *Sci. Total Environ.* **651**, 2228-2234.
1133 Wells, N.S., Baisden, W.T., Horton, T. and Clough, T.J. (2016) Spatial and temporal variations in
1134   nitrogen export from a New Zealand pastoral catchment revealed by stream water nitrate
1135   isotopic composition. *Water Resour. Res.* **52**, 2480-2854.
1136 Wells, N.S. and Eyre, B.D. (2019) $\delta^{15}N$ patterns in three sub-tropical estuaries show switch from
1137   nitrogen 'reactors' to 'pipes' as degradation increases. *Limnol. Oceanograph.* **64**, 860-876.
1138 Wells, N.S., Maher, D.T., Huang, P., Erler, D.V., Maxwell, P., Hipsey, M.R. and Eyre, B.D. (2020)
1139   Land-use intensity alters both the source and fate of CO_2 within eight sub-tropical estuaries.
1140   *Geochim Cosmochim Ac* **268**, 107-122.
1141 Wickham, H. (2016) ggplot2: Elegant Graphics for Data Analysis. Springer-Verlag New York,
1142   https://ggplot2.tidyverse.org.
1143 Wollheim, W.M., Bernal, S., Burns, D.A., Czuba, J.A., Driscoll, C.T., Hansen, A.T., Hensley, R.T.,
1144   Hosen, J.D., Inamdar, S., Kaushal, S.S., Koenig, L.E., Lu, Y.H., Marzadri, A., Raymond,
1145   P.A., Scott, D., Stewart, R.J., Vidon, P.G. and Wohl, E. (2018) River network saturation

1146   concept: factors influencing the balance of biogeochemical supply and demand of river
1147   networks. *Biogeochem.* **141**, 503-521.
1148 Wu, S., Chen, J., Li, C., Kong, D.L., Yu, K., Liu, S.W. and Zou, J.W. (2018) Diel and seasonal
1149   nitrous oxide fluxes determined by floating chamber and gas transfer equation methods in
1150   agricultural irrigation watersheds in southeast China. *Environ. Monit. Assess.* **190**, 14.
1151 Xia, X.H., Liu, T., Yang, Z.F., Michalski, G., Liu, S.D., Jia, Z.M. and Zhang, S. (2017) Enhanced
1152   nitrogen loss from rivers through coupled nitrification-denitrification caused by suspended
1153   sediment. *Sci. Total Environ.* **579**, 47-59.
1154 Xu, M.N., Li, X.L., Shi, D.L., Zhang, Y., Dai, M.H., Huang, T., Glibert, P.M. and Kao, S.J. (2019)
1155   Coupled effect of substrate and light on assimilation and oxidation of regenerated nitrogen in
1156   the euphotic ocean. *Limnol. Oceanograph.* **64**, 1270-1283.
1157 Yang, X.Q., Jomaa, S., Buttner, O. and Rode, M. (2019) Autotrophic nitrate uptake in river networks:
1158   A modeling approach using continuous high-frequency data. *Water Res* **157**, 258-268.
1159 Yoshida, N. and Toyoda, S. (2000) Constraining the atmospheric N_2O budget from intramolecular site
1160   preference in N_2O isotopomers. *Nature* **405**, 330-334.
1161 Zarnetske, J.P., Haggerty, R., Wondzell, S.M., Bokil, V.A. and Gonzalez-Pinzon, R. (2012) Coupled
1162   transport and reaction kinetics control the nitrate source-sink function of hyporheic zones.
1163   *Water Resour. Res.* **48**, 15.

1164